SAPIENZA
University of Rome
Faculty of Pharmacy and Medicine

PhD Programme in
Morphogenesis and Tissue Engineering

31st Cycle
(A.A. 2015/2016 - 2017/2018)

Development Of a Biological Scaffold From Adult Human Skin For Cardiovascular Repair and Regeneration

PhD student
Clotilde Castaldo

Tutor
Prof. Stefania Montagnani

Coordinators
Prof. Sergio Adamo
Prof. Antonio Musarò

CONFIDENTIALITY NOTICE

Reviewers and PhD committee members are obliged to keep the files confidential and to delete all records after completing the review process.

Il ricevimento degli elaborati scientifici, per l'ottenimento del titolo di Dottore di Ricerca, in qualità di Membro del Collegio dei Docenti del Dottorato in Morfogenesi ed Ingegneria Tissutale richiede di osservare le seguenti normative:

i. considerare le Informazioni confidenziali e riservate come strettamente private e ad adottare tutte le ragionevoli misure finalizzate a mantenerle tali;

ii. utilizzare le Informazioni confidenziali e riservate unicamente allo scopo per le quali sono state fornite o rese note, impegnandosi a non divulgarle a soggetti terzi le informazioni contenute negli elaborati ricevuti;

iii. a garantire la massima riservatezza, anche in osservanza alla vigente normativa in materia di marchi, di copyright e di brevetti per invenzioni industriali e in base alla normativa sulla privacy, ai sensi del D.Lgs. 196/2003, riguardo il know-how e tutte le informazioni acquisite, che non potranno in alcun modo, in alcun caso e per alcuna ragione essere utilizzate a proprio o altrui profitto e/o essere divulgate e/o riprodotte o comunque rese note a soggetti terzi.

Index

The thesis explained

Cardiovascular diseases (CVDs) are still the leading cause of death and disabilities globally. Among CVDs, ischemic heart disease (IHD) has remained the leading cause of death worldwide in the last 16 years. IHD is caused by a sudden blockage of blood flow through coronary arteries that prevents the supply of oxygen and nutrients to the region of myocardium fed by the affected vessels. This condition causes the necrosis of the myocardium that is followed by a reparative process that starts from the infarcted area, but then involves, at later stages, also the uninjured myocardium, causing progressive fibrosis that may lead eventually to heart failure. Unfortunately, there is no cure for IHD and therapy can at best control symptoms and prevent a second ischemic event. The induction of post-infarction cardiac regeneration by the means of three factors, cells, scaffold and signals, is currently the target of cardiac tissue engineering. However, the field is still at its infancy and all three factors are yet to be defined. Since the ECM is the naturally occurring scaffold loaded with uncountable biological and mechanical signals, we aimed at obtaining and characterizing a biological three-dimensional scaffold for cardiac repair and regeneration from the adult human skin.

Our results provided evidence that the scaffold of decellularized human skin (d-HuSk) was acellular and had a preserved architecture, retained components of the ECM that are also typical of cardiac matrix and are critical for cardiac functions and mechanical properties of the ECM, like collagen, fibronectin, laminin, tenascin, elastin and GAGs. Additionally, growth factors stored in d-HuSk matrix were similar to those found in cardiac matrix and, as similar were the signals, similar were the effects of d-HuSk and cardiac matrix on human cardiac progenitor cells (hCPCs). Indeed, as emerged from cytocompatibility study, the environment offered by d-HuSk did not differ from the cardiac native one in supporting engraftment and survival of hCPCs. Furthermore, d-HuSk attracted hCPCs from the cardiac native

matrix and sustained their differentiation and differentiation towards cardiac myocytes.

Therefore, d-HuSk is a biological scaffold that is easily obtained and might be used as an autograft. It shares to a large extent the composition of the cardiac native matrix, exerts on hCPCs similar effects *in vitro* and is also capable of stimulating their mobilization and engraftment. Overall, d-HuSk fulfills the key requirements needed for a scaffold to warrant its use in tissue engineering and, then, holds great promise as substitute for cardiac environment. Additionally, consisting of ECM proteins and being a storage of growth factors, d-HuSk might alone provide two of the three pillars of tissue engineering, namely the scaffold and the signals, and might be exploited as stand-alone scaffold to boost cardiac regeneration by recruiting resident cardiac progenitor cells, or as a cellularized scaffold by preparing a cardiac engineered tissue *in vitro* with the cell population of choice.

List of Abbreviations

ACE	Angiotensin-Converting Enzyme
ACTC	Cardiac muscle Actin
ANOVA	Analysis of Variance
bFGF	basic Fibroblast Growth Factor
BMMNCs	Bone Marrow-derived Stem Cells
CA	California
CABG	Coronary Artery Bypass Graft (CABG)
CAD	Coronary Artery Disease
CDCs	Cardiosphere-Derived Cells
CPCs	Cardiac Progenitor Cells
CVDs	Cardiovascular Diseases
CX	Connexin
DAB	Diaminobenzidine
DALY	Disability-Adjusted Life Year
DAPI	4',6-diamidino-2-phenylindole
d-HuM	decellularized Human Myocardium
d-HuSk	Decellularized Human Skin
DNA	Deoxyribonucleic acid
dsDNA	Double-stranded Deoxyribonucleic acid
ECM	Extracellular Matrix
EDTA	Ethylenediaminetetraacetic Acid
EGF	Epidermal Growth Factor
ESCs	Embryonic Stem Cells
F12K	Nutrient Mixture F-12 Ham
FBS	Fetal Bovine Serum
FESEM	Field-Emission SEM
GA	Georgia
GAGs	Glycosaminoglycans

GAPDH	Glyceraldehyde 3-phosphate dehydrogenase
GMCSF	Granulocyte-Macrophage Colony-Stimulating Factor
H&E	Hematoxylin and Eosin
HBSS	Hank's Balanced Salt Solution
hCPCs	Human Cardiac Progenitor Cella
HGF	Hepatocyte Growth Factor
HRP	Horseradish Peroxidase
HuM	Human Myocardium
IGF	Insulin-like Growth Factor
IHD	Ischemic Heart Disease
iPSCs	induced Pluripotent Stem Cells
MA	Massachusetts
MACS	Magnetic-Activated Cell Sorting
MD	Montana
MEF	Myocyte-specific Enhancer Factor
MI	Myocardial Infarction
MO	Missouri
MSCs	Mesenchymal Stem Cells
MYH	MutY homolog
NCDs	Non-Communicable Diseases
NJ	New Jersey
PBS	Phosphate Buffer Saline
PCI	Percutaneous Coronary Intervention
PCR	Polymerase Chain Reaction
PDGF	Platelet-Derived Growth Factor (PDGF)
RNA	Ribonucleic Acid
SCF	Stem Cell Factor
SDS	Sodium Dodecyl Sulfate
SEM	Scanning Electron Microscope

SEM	Standard Error of Mean
SMs	Skeletal Myoblasts
TBX	T-box
TGF-beta	Transforming Growth Factor (bFGF)
UK	United Kingdom
USA	United States of America
VEGF	Vascular Endothelial Growth Factor
VT	Vermont
WA	Washington
WHO	World Health Organization
YLDS	Years of Life Lived with Disability
YLLs	Years of Life Lost

1 Introduction

1.1 Cardiovascular diseases

1.1.1 Definition

Cardiovascular diseases (CVDs) are disorders of the heart and blood vessels that include coronary heart disease, cerebrovascular disease, peripheral arterial disease, rheumatic heart disease, congenital heart disease and deep vein thrombosis and pulmonary embolism (1). CVDs and other chronic diseases like chronic respiratory diseases and diabetes are classified by World Health Organization (WHO) as non-communicable diseases (NCDs).

1.1.2 Epidemiology and risk factors

Based upon WHO computations, NCDs are responsible every year for 41 million deaths that account for 71% of all deaths globally (2). Remarkably though, cardiovascular diseases (CVDs), cancers, chronic respiratory diseases, and diabetes collectively account for 70% of all NCD deaths, while CVDs alone are responsible for 31% of all deaths worldwide (1). Furthermore, CVDs are major contributors to overall disease burden, expressed as the disability-adjusted life year (DALY), which is a measure of both the quality of life and the life expectancy of affected patients expressing the number of years of life lived with disability (YLDs) and years of life lost (YLLs) due to ill-health.

Among CVDs ischemic heart disease (IHD) was responsible for more than 15% of all deaths in all countries from the low-income to the high-income economies in 2016. Although most IHD deaths can be prevented or delayed by addressing behavioral risk factors, they continue to be an important public health challenge in all countries and IHD has remained the leading cause of death in countries ranging from lower-middle to high income in the last 16 years (Fig. 1) (3).

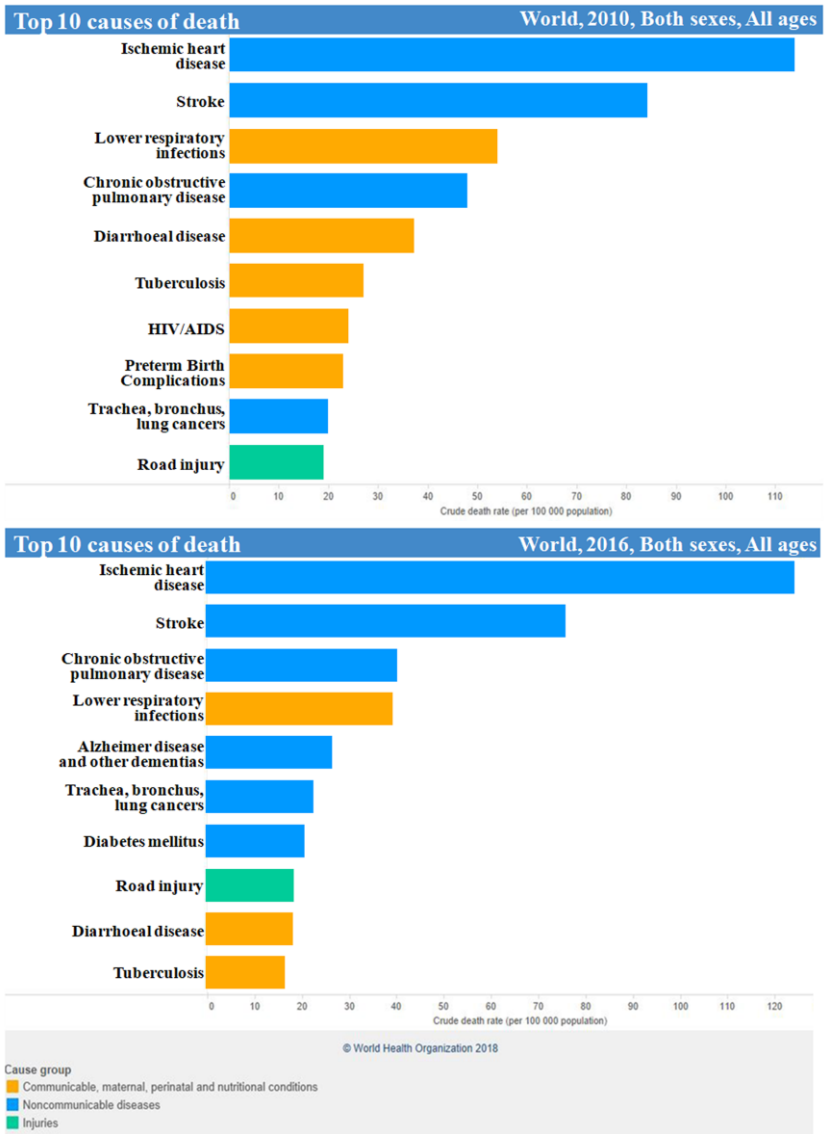

Figure 1. Top 10 causes of death worldwide. Major causes of death globally in 2000 (graph on the top) and in 2016 (graph on the bottom). Ischemic heart disease has remained the leading cause of death worldwide for the last 16 years (http://www.who.int/news-room/fact-sheets/detail/the-top-10-causes-of-death).

However, this difference is likely due to the great variation in life expectancy, since people from poorer countries die from other conditions before reaching an age where they would develop IHD (4).

Behavioral risk factors, including tobacco use (5), unhealthy diet (6), lack of physical activity (7) and the harmful use of alcohol (8), lead in turn to obesity, diabetes, hypertension and high blood cholesterol (9). All these conditions dramatically increase the risk of developing CVDs (10-13). Hence, the burden of IHD can be effectively reduced by tackling modifiable behavioral risk factors (14). Governments have made strong political commitment to implement measures to reduce the harmful use of alcohol and to promote healthy diet and physical activity and to strengthen health systems through primary health care and universal health coverage interventions aimed at promoting and supporting healthier lifestyle. However, although the progress was tangible in western countries (15-17), it has been highly uneven. In fact, the burden of IHD is rising disproportionately among low-income and lower-middle-income countries, due to other important risk factors like poverty, psychosocial status (18), low educational status, globalization of food industry, rapid urbanization and population growth (19).

1.2 The Ischemic Heart Disease (IHD)

IHD is due to coronary artery disease (CAD), a condition characterized by the formation of the atherosclerotic plaque within the wall of the vessels that feed the myocardium, namely the coronary arteries (Fig. 2, A). This process, termed atherosclerosis, occurs through the gradual accumulation of lipids in the vessel wall and involves inflammatory cells, endothelial cells and smooth muscle cells (20). Eventually, the plaque in a carotid artery hardens or ruptures and causes reduction or interruption of blood flow whose clinical manifestation is IHD.

Myocardial infarction (MI) occurs when the blood flow is suddenly blocked more often due to the formation of a clot on a

ruptured atherosclerotic plaque. This blockage prevents the supply of oxygen and nutrients to the region of myocardium supplied by the affected arterial branch. If this condition persists it leads inexorably to the death of cardiac myocytes (Fig. 2, B).

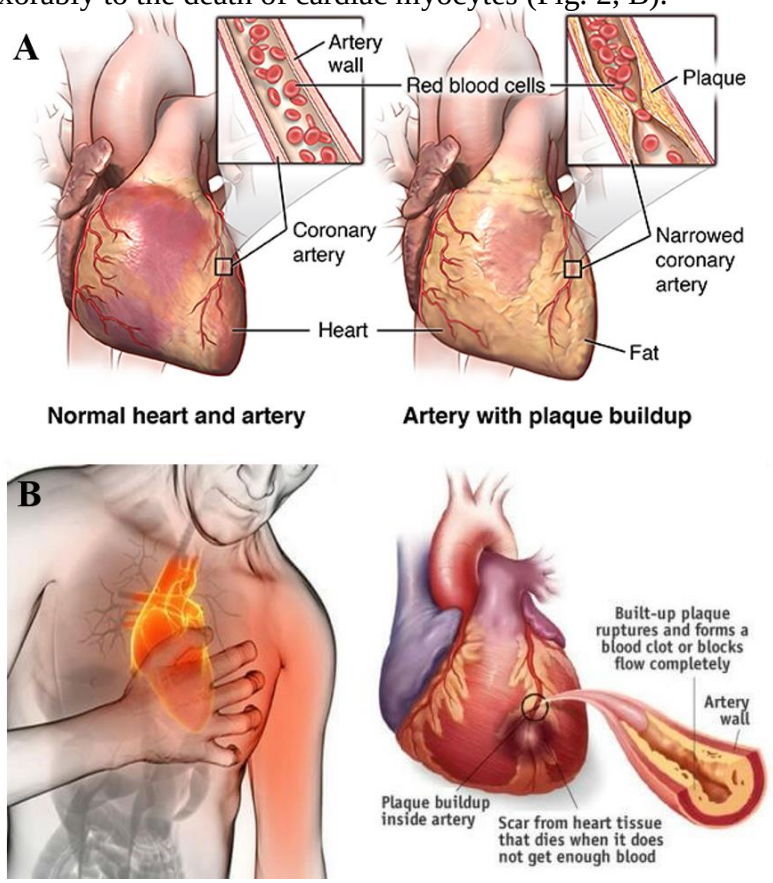

Figure 2. Coronary Artery Disease and Ischemic Heart Disease. Coronary artery disease is characterized by the formation of the atherosclerotic plaque within the wall of coronary artery (A). More often the myocardial infarction is caused by the rupture of a plaque and the formation of a clot that blocks the blood flow and prevents the supply of oxygen and nutrients to the myocardium fed by the involved vessel (B).

Due to the sudden ischemic death of cardiac myocytes as to the very limited regenerative ability of human myocardium, cardiac tissue damage triggers a series of complex events that leads to the reorganization of cardiac extracellular matrix (ECM) at site of injury and to the replacement of dead myocardium with permanent scar tissue. Such "local" early remodeling that involves the infarcted area occurs as a beneficial response to prevent ventricular wall rupture and is referred to as reparative or replacement fibrosis (Fig. 3). Specifically, tissue injury causes the releases of endogenous molecules known as alarmins (21) that are involved in cardiac repair by eliciting an inflammatory response that clears the necrotic area of degraded ECM and of dead cells. Furthermore, the release of soluble factors, like IL-1, IL-6 and TGF-beta 1, causes the activation of cardiac fibroblasts and their transdifferentiation to myofibroblasts (22) that synthesize and secrete large quantities of ECM proteins, including type I collagen, fibronectin, and tenascin C (23, 24). The formation of scar stabilizes the infarcted zone and the region immediately adjacent to it, but it also causes a dilation (25). However, cardiac remodeling following MI causes geometric changes that involve both the infarcted and non-infarcted myocardium (26, 27). Indeed, replacement fibrosis is followed by the remodeling of border zone and remote uninjured myocardium, where myocytes undergo hypertrophy in response to an unbalanced distribution of wall stress and ECM undergoes extensive rearrangement with excessive deposition of type I collagen, at the expense of the much less rigid type III collagen, to stabilize heart chambers and prevent further deformation. Such fibrotic response involves the left ventricle globally and is referred to as reactive or interstitial fibrosis (28) (Fig. 4).

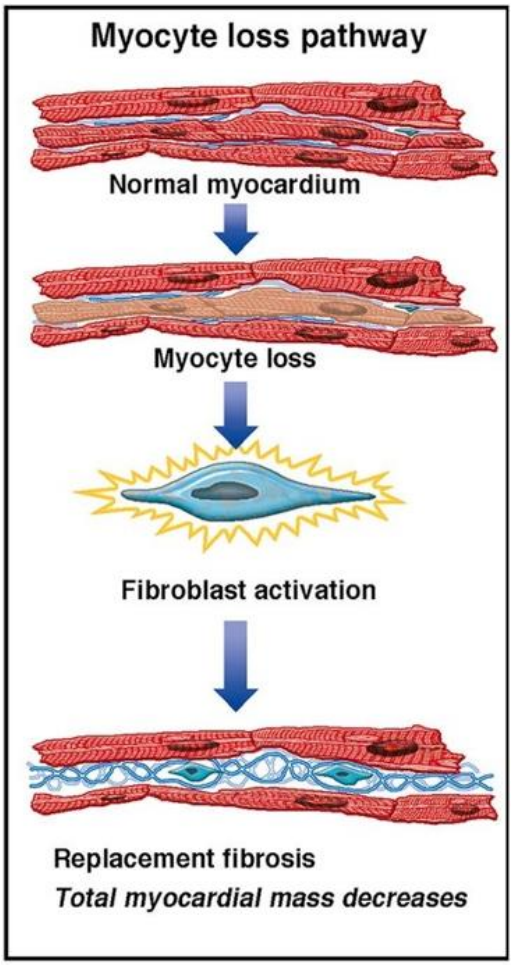

Figure 3. Reparative or replacement fibrosis occurring after MI. Due to massive myocyte death, activated fibroblasts transdifferentiate into myofibroblasts, whose synthesis and deposition of a collagen-rich ECM leads to the replacement fibrosis (from JACC 2014;63:2188-2198).

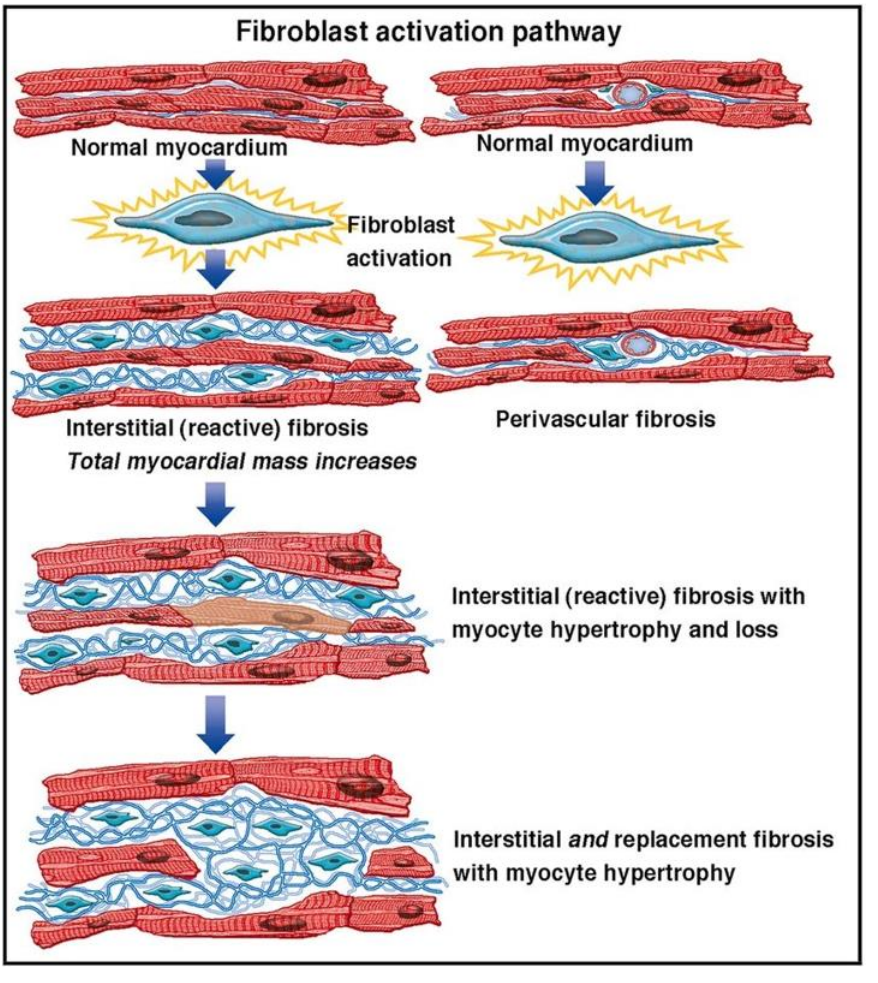

Figure 4. Compensatory cardiac remodeling of the remote myocardium leads to the reactive fibrosis. The reparative fibrosis causes ventricular geometric changes that are responsible for an uneven distribution of mechanical forces through the myocardium. Healthy myocytes in regions remote to the infarcted area respond to such modified mechanical stimulation by undergoing hypertrophy, while fibroblasts are activated and synthesize excessive collagen. This fibrotic response, termed reactive or interstitial fibrosis, involves the left ventricle globally (from JACC 2014;63:2188-2198).

This progressive fibrosis occurring in the myocardium remote to the infarcted region disrupts myocardial architecture and have adverse effects on ventricular function (29). Therefore, the inflammatory response that is essential for cardiac repair is also implicated in the pathogenesis of post-infarction remodeling and may eventually lead to heart failure (30), a complex clinical syndrome caused by a structural or functional cardiac disorder that results in systolic or diastolic dysfunction responsible, in turn, for heart inability to perform sufficient pumping to meet body's needs (31, 32).

1.3 Current Treatment of IHD

Lifestyle changes, drugs, and medical procedures can help prevent or treat coronary heart disease.

The initial therapy of MI is directed toward restoration of perfusion as soon as possible to limit myocyte loss. This may be accomplished through a pharmacological fibrinolysis in selected patients or by mechanical means, such as percutaneous coronary intervention (PCI), or coronary artery bypass graft (CABG) surgery.

Successively, pharmacological therapy aimed at reducing mortality, relieve symptoms and signs, improve quality of life, prevent the occurrence of further myocardial damage and the remodeling of the myocardium is established.

The medical therapy relies on several drugs, including anti-thrombotic agents, vasodilator agents, beta-adrenoceptor antagonists (beta blockers), statins, diuretics, aldosterone receptor antagonists, angiotensin-converting enzyme (ACE) inhibitors, angiotensin II receptor blockers, whose combinations are dictated by the course of the disease and clinical conditions of the patients, as evaluated by follow-up (31-33).

Albeit considerable advances achieved in the understanding of the pathologic mechanisms of cardiac disease, modern therapies remain not curative, since the problem of cardiomyocyte loss has not yet been solved (34) and treatment can at best help to relieve

symptoms, reduce myocardial remodeling and the risk of having another ischemic event.

As a result, the induction of post-infarction cardiac regeneration in adult mammals is currently the target of intensive research and drug discovery attempts.

1.4 Future Treatment of IHD

Regenerative medicine is aiming at restoring structure and function of damaged tissues and organs. The goal of this approach rises from the needing to develop a strategy to treat previously incurable injuries and highly deadly pathologies, as cardiovascular diseases (35). A combination of approaches and tools, such as tissue engineering, cellular therapies, and medical devices or artificial organs can enhance the healing process naturally occurring in human body as result of an injury (36). The close cooperation of diverse fields, like biology, chemistry, tissue engineering and even robotics is required to deal with such a challenging task (37).

1.4.1 Cardiac Cell Therapy

Cell therapy has been experimented for more than a decade, with a number of cell types used in clinical trials in seeking to replace damaged cells or to repair injured tissue (38).

A pioneer study with the first cells used for cardiac regeneration, was performed in 1998 by Taylor et al. and demonstrated that skeletal myoblasts (SMs) have the ability to enhance and partially restore cardiac function (39). This study was an inspiration for the further use of many other cell types, such as bone marrow-derived stem cells (BMMNCs) (40-43), Mesenchymal stem cells (MSCs) (43), cardiac progenitor cells (CPCs) (44), cardiosphere-derived cells (CDCs) (45, 46), embryonic stem cells (ESCs) (47) and more recently induced pluripotent stem cells (iPSCs) (48, 49). There are still more controversies about the use of cells in therapy: on one hand they

produced encouraging results in improving the global cardiac function, and this is probably due to a paracrine action more than an effective integration and proliferation or survival *in vivo*, on the other hand the results of pre-clinical studies conducted in animal models and clinical trials conducted in humans were variable, not reproducible, and a number of obstacles and side effects were frequent (38).

One of the major obstacles about cell therapy was to find the appropriate way to deliver a sufficient number of cells to the damaged area in the less invasive way (34). Intracoronary and intramyocardial injection after myocardial infarction were the preferred strategies, even if the integration, the engraftment and the long-term survival of cells administrated was very weak (50).

An alternative to the direct injection of cells is the implantation of engineered tissue to offer a both mechanical and biological support to enhance cell retention and function *in vivo* (51).

1.4.2 Cardiac Tissue Engineering

Tissue engineering technologies aim at the generation of three-dimensional tissue-like scaffolds for therapeutic use. Three factors are pivotal for a successful approach: cells, extracellular matrix, and biomimetic signals (52) (Fig. 5).

Scaffolds, in fact, require specific features to produce the desirable therapeutic outcome, as they have to guide cell organization, growth and differentiation, and have to ensure structural stability and a suitable environment where cells can produce new biological tissue (53).

Biocompatibility, biodegradability and appropriate mechanical properties are the major criteria used for the production of an engineered biological construct (52).

Biocompatibility is needed to avoid immune reactions undesirable for patients, and because cells must be attracted by the construct in order to adhere, proliferate and migrate like in a normal or natural microenvironment (54).

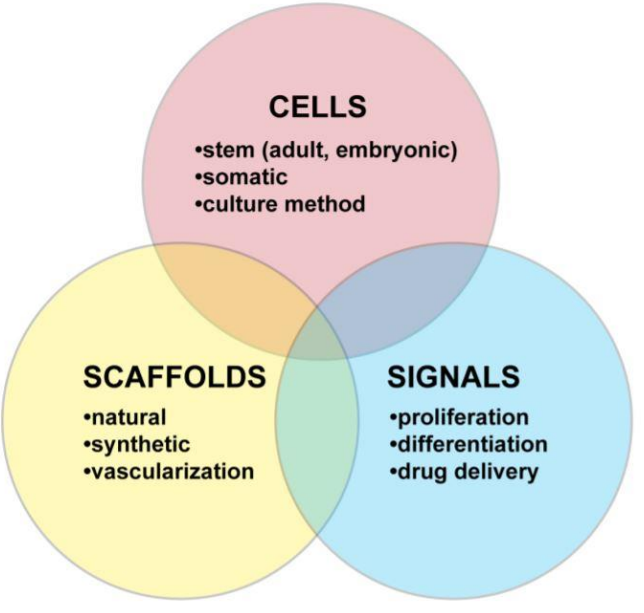

Figure 5. The tissue engineering triad. Tissue engineering strategies are based on three pillars: cells to rebuild the tissue, scaffolds to recreate the tissue environment and physical and chemical signals to support and stimulate cellular functions.

A scaffold must be non-permanent and for this reason, biodegradability is a notable characteristic. In fact, once cells begin to produce their own new and healthy extracellular matrix, the scaffold is no more needed (52).

It is crucial to customize the scaffold depending on the anatomical site of destination, in particular, mechanical properties and architecture must be balanced to guarantee the surgical handling during the implantation procedure and the adequate porosity to allow cell infiltration and vascularization (52).

Several biomaterials, either natural or synthetic, have been tested thus far as substitute for cardiac environment to support cell-based regeneration (55).

However, on the one hand the spatial organization of structural ECM components and the biochemical complexity of the ECM can be fully recapitulated only by the naturally occurring cardiac ECM, but, on the other hand, biomaterials are tunable in their physical properties that have been demonstrated to drive stem cell differentiation and behavior (56). Therefore, finding a substitute able to recapitulate, at least partially, mechanical and biological features of the myocardium is a primary goal in cardiac regenerative medicine.

2 Aims

Cardiac cell therapy demonstrated that regeneration cannot occur without restoring the extracellular compartment along with the cellular compartment, as cell death causes a dramatic rearrangement of myocardial environment that triggers the replacement fibrosis and sustains the reactive fibrosis. The replacement of noncompliant scar tissue with newly formed and fully functional myocardium in the infarcted region would compensate the limited regenerative ability of human adult myocardium and oppose the pathological remodeling that inexorably takes place in the remote region of the ischemic heart.

Cardiac tissue engineering promise to heal the infarcted heart relies on the combination of a scaffold with growth factors and cells. Scaffold and growth factors are employed to restore the microenvironment in its composition, architecture and signaling activity, while cells are needed to form new vessels and replace cardiac supporting and parenchymal cells.

The aim of this study is to explore *in vitro* the possibility of constructing a three-dimensional scaffold for cardiac repair and regeneration from the adult human skin. The skin is the largest organ in the body that can be easily and opportunely harvested to provide a viable biological and autologous substitute for cardiac environment. Furthermore, cardiac and dermal ECMs are rich in collagen, laminin and elastin. Therefore, the decellularized human skin may also provide biological signals and mechanical properties, like elasticity, that are, at least partially, shared with the microenvironment of the myocardium. Based on the mounting evidence that the adult human heart hosts a population of resident cardiac progenitor cells, a scaffold carrying biological and mechanical signals might yet be used as stand-alone bioengineering product.

To test our hypotheses, we prepared biological scaffold of decellularized human skin (d-HuSk) and decellularized human myocardium (d-HuM). Then, we evaluated whether d-HuSk

showed promise to serve as substitute for cardiac environment by analyzing its composition, biocompatibility and capability of delivering biological signals like the signals delivered by the native cardiac environment. Moreover, we analyzed *in vitro* the effects of d-HuSk on the engraftment and differentiation of resident cardiac progenitor cells to assess the potential of d-HuSk to serve as both cell-delivering and stand-alone scaffold.

3 Results and discussion

3.1 The decellularization of human skin from living subjects can be swiftly and efficiently accomplished

To be considered suitable for regenerative medicine applications, scaffolds of decellularized matrix should not elicit an immune response. This implies that decellularization process should ensure a complete removal of cellular antigens (57, 58). The currently accepted criteria to satisfy the intent of decellularization include a residual double-stranded DNA (dsDNA) content of less than 50 ng dsDNA per mg of dry decellularized tissue and lack of visible nuclear material in tissue sections stained with Hematoxylin and Eosin (H&E) (59). Snap-frozen skin samples were decellularized following a recently published protocol proven successful for a fast and effective decellularization of human myocardium (60). The first obvious change that occurred with the decellularization was in the color of samples that turned completely white with the respect to the brownish color of native skin (Fig 6, A and B). Then quantitative measurements of DNA content and H&E staining were used to evaluate the effectiveness of decellularization and suitability of d-HuSk as biological scaffold for tissue engineering, in accordance to aforementioned criteria. Analysis of DNA content clearly showed the virtual absence of dsDNA in d-HuSk (Fig 6, C), whose residual amounts were well below the currently accepted standard resulting as low as 7.50 ± 2.162 ng per mg of dry tissue (Fig 6, B). Such dramatic result was confirmed by the histological analysis as H&E staining demonstrated the absence of nuclei in d-HuSk (Fig. 6, F) when compared with native skin (Fig. 6 E). Notably though, decellularization might be a very harsh treatment for soft tissues. The combination of chemical and mechanical methods of decellularization can cause both a biological impoverishment of the ECM and a disruption of tissue integrity and architecture (61).

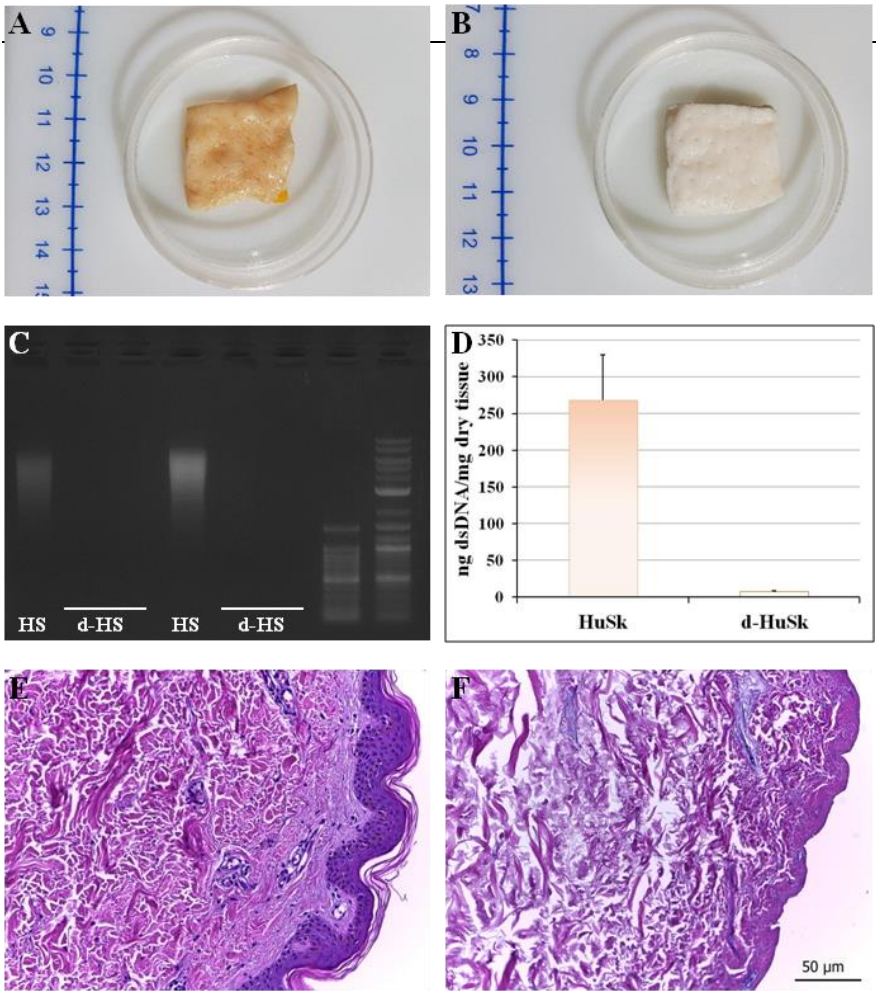

Figure 6. Evaluation of the effectiveness of the decellularization procedure of skin. A and B: Representative images of macroscopic examination of native human skin (HuSk) (A) and decellularized human skin (d-HuSk) (B) showing an obvious change in color, inasmuch as d-HuSk samples were completely white. C and D: Representative gel electrophoresis revealing an extremely low content of residual dsDNA in d-HuSk (n = 6) with bands barely visible (C) and concentration of DNA well below that of the native skin (n = 4) and the proposed criterion of 50 ng (D). Data are expressed as mean ± SEM. (HS: native human skin, d-HS: d-HuSk). E and F: representative H&E image comparing native human skin (E) with d-HuSk (F) and confirming the effectiveness of decellularization as shown by the absence of nuclei in d-HuSk. (Scale bar: 50 µm).

Therefore, it is crucial to find the right balance between strength, to ensure the complete removal of cells and debris, and subtlety, to avoid marked alteration of native structure and composition of matrix. Indeed, the histological analysis showed an overall well-preserved architecture of the dermal matrix in d-HuSk (Fig 6, F). Therefore, d-HuSk not only fulfilled the requirements proposed for the evaluation of the effectiveness of decellularization, but also preserved the histological organization of native tissue, providing compelling evidence of a highly efficient decellularization method.

3.2 Decellularized Human Skin (d-HuSk) consists of structural and functional ECM proteins that are key components of the cardiac matrix

The ECM is a complex network of fibrous proteins, polysaccharides and soluble factors. On the one hand, the ECM is continuously produced and remodeled by resident cells, but, on the other hand, its unique composition and three-dimensional organization provide biological and mechanical cues that are responsible for directing stem cell fate (62) and cell behavior both in physiological and pathological states. Unquestionably, the ideal scaffold for cardiac regeneration would be the naturally occurring cardiac ECM and the most ambitious - and still unmet - aim of cardiac tissue engineering is to replicate its architecture and composition. Aiming at investigating on the suitability of d-HuSk as substitute for cardiac ECM, we evaluated by immunohistochemistry the presence and localization in d-HuSk of structural and non-structural proteins of the ECM (63) that are described as main components of both cardiac (64) and dermal matrix (65, 66) and that we previously reported as retained by decellularized cardiac matrix (60).

Immunohistochemical analysis revealed that type I, III and IV collagens (Fig. 7) and the non-collagenous proteins, like fibronectin, laminin and tenascin (Fig. 8), were preserved in d-HuSk as well. Type I and III collagens resulted scattered throughout the entire dermis (Fig. 7, A-D), along with fibronectin

(Fig. 8, A-B) and tenascin (Fig. 8, E-F), while type IV collagen (Fig. 7, F) and laminin (Fig. 8, D) were localized mostly in the basement membrane of vessels. Moreover, type III collagen (Fig. 7, D) and tenascin formed a delicate texture (Fig. 8, F), while type I collagen (Fig. 7, B) and fibronectin (Fig. 8, B) were visible as thicker bundles.

The investigated ECM components are the main structural and functional proteins of cardiac matrix and their retention in d-HuSk provide evidence to substantiate the ability of d-HuSk to deliver a combination of structural support and biological signals that act in cardiac microenvironment. Specifically, fibril-forming type I and III collagens are the main collagenous component of the cardiac matrix (67) that provide tensile strength and are responsible for the integrity of cardiac interstitial connective tissue. Additionally, type I collagen promotes cardiomyogenesis of MSCs (68, 56), while fibronectin, laminin and tenascin, other than playing major role in cell adhesion and migration or in tissue repair, are involved in embryonic development of the heart (69-71). Particularly, fibronectin is required during cardiac morphogenesis for the formation of the cardiac outflow tract and nodes and it is involved in the differentiation of neural crest cells into vascular smooth muscle cells by regulating Notch signaling (72), tenascin C is transiently expressed during the development of the heart at restricted sites to promote differentiation of cardiomyocytes (73), while laminin in the developing heart orchestrates the assembly of the cardiac ECM and in the adult heart lines the myocardial cells (74). Such functions are collectively of strategic importance when considering the application of d-HuSk in a stem cell-based cardiac regeneration approach, conferring to d-HuSk the potential to support and boost cardiac differentiation.

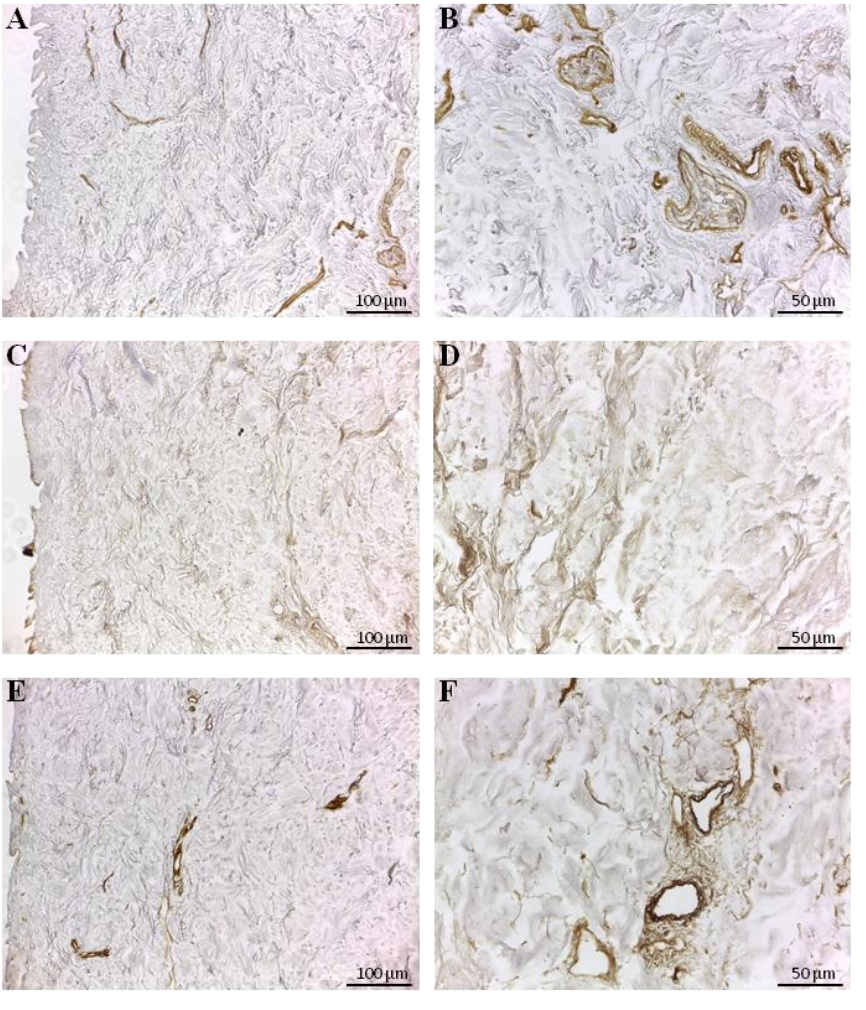

Figure 7. Immunodetection of collagen type I, III and IV in d-HuSk. Representative images of the immunohistochemical analysis showing the presence and localization of the main cardiac collagenous components in d-HuSk: the fibrillar type I (A, B) and III (C, D) collagen and the collagen type IV (E, F) with its typical localization in the basement membrane. (Scale bar: 100 µm for A, C and E, and 50 µm for B, D and F).

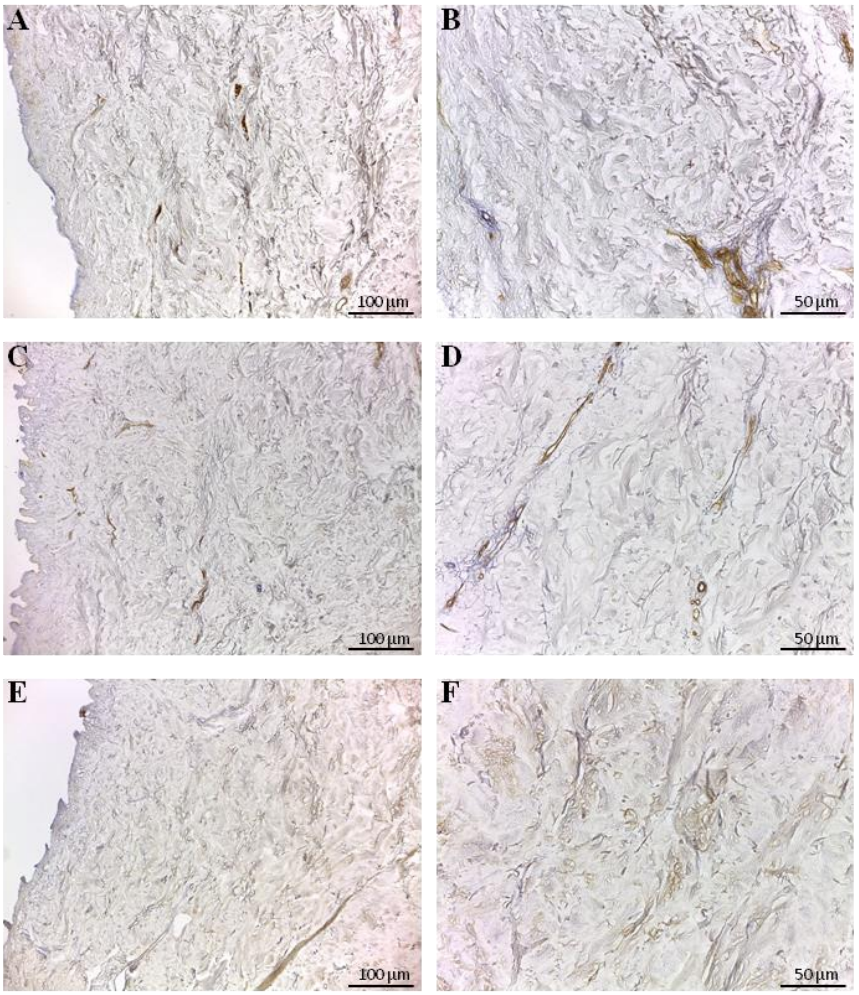

Figure 8. Immunodetection of fibronectin, laminin and tenascin in d-HuSk. Representative images of the immunohistochemical analysis showing the presence and distribution of fibronectin (A, B), laminin (C, D) and tenascin (E, F) in d-HuSk. (Scale bar: 100 µm for A, C and E, and 50 µm for B, D and F).

3.3 d-HuSk has the potential to deliver mechanical stimuli

When evaluating biological scaffold for regenerative medicine applications it is crucial to focus on the main requirements that the bioconstruct must fulfil to be eventually translated to the clinics. As for myocardium, along with the biochemical cues regulating cellular processes, like proliferation, differentiation and apoptosis, muscle cells need a compliant matrix that allows contraction and relaxation cycles while preserving its integrity. Hence, mechanical properties of scaffolds should be considered as important as biological signals.

Other than collagens, also elastin and glycosaminoglycans (GAGs) are known to be responsible for the biomechanical properties of ECM (75, 76). Particularly, elastin is the dominant mammalian elastic protein and, as the main component of elastic fibers, is responsible for tissue flexibility (77), while glycosaminoglycans (GAG) are highly hydrophilic chains of proteoglycans whose significant water-binding capacity confers mechanical stability to tissues (78).

Therefore, we analyzed the retention and distribution of elastin and GAGs in d-HuSk by Paraldehyde fuchsin Gomori's, Weigert Van Gieson and Alcian Blue stainings. Then we performed comparative analysis between d-HuSk and adult human myocardium by quantitative dye-binding assay for elastin and GAG content to gain an insight into what might be the mechanical properties of d-HuSk with the respect to human myocardium (79).

Paraldehyde fuchsin Gomori's (Fig. 9, A and B) and Weigert Van Gieson (Fig. 9, C and D) stainings clearly showed the presence of elastic fibers in native skin (Fig. 9, A and C), and in d-HuSk (Fig. 9, B and D), where the retention of elastic fibers surrounding well-preserved blood vessels resulted glaringly obvious (Fig. 9, B and D, red and yellow arrowheads, respectively). Quantitative Fastin Elastin assay not only confirmed the presence of elastin in d-HuSk but showed also that elastin

content of d-HuSk did not differ significantly from the elastin content of native skin 34,2054 ± 2,529 µg/mg of dry tissue in d-HuSk vs. 37,5772 ± 2,561 µg/mg of dry tissue in HuSk) (Fig. 8, E).

Similarly, Alcian Blue staining revealed the presence of GAGs in native skin (Fig. 10, A), and in d-HuSk (Fig. 10, B), while quantitative Blyscan assay confirmed the retention by d-HuSk of amounts of GAGs that did not differ significantly from the content of native skin (76,89 ± 14,22 µg/mg of dry tissue vs. 100,7 ± 17,36 µg/mg of dry tissue in HuSk) (Fig. 10, C).

Conversely, the content of elastin and GAGs differed between human myocardium and d-HuSk. Indeed, native human myocardium contained significantly ($p < 0.05$) higher amount of elastin when compared to d-HuSk (116,50 ± 6,499 µg/mg of dry tissue vs. 34,2054 ± 2,529 µg/mg of dry tissue). Interestingly though, the elastin content of d-HuSk did not differ significantly from that of d-HuM (34,2054 ± 2,529 µg/mg of dry tissue vs 48,18 ± 9,629 µg/mg of dry tissue) (Fig. 11, A). Although the difference observed between d-HuSk and native myocardium must be taken into account when evaluating the overall composition of d-HuSk, it is of note that, as far as we are concerned, the best substitute for cardiac ECM in terms of composition is the decellularized cardiac ECM. Therefore, the comparison between d-HuSk and d-HuM is more appropriate to assess the suitability of d-HuSk as a scaffold for cardiac regenerative medicine. As regards GAGs, instead, quantitative analysis revealed a significantly ($p < 0.001$) lower content of GAGs in both native (18,69 ± 2,344 µg/mg of dry tissue) and decellularized (12,60 ± 2,300 µg/mg of dry tissue) human myocardium, when compared with the content of d-HuSk (76,89 ± 14,220 µg/mg of dry tissue) (Fig. 11 B).

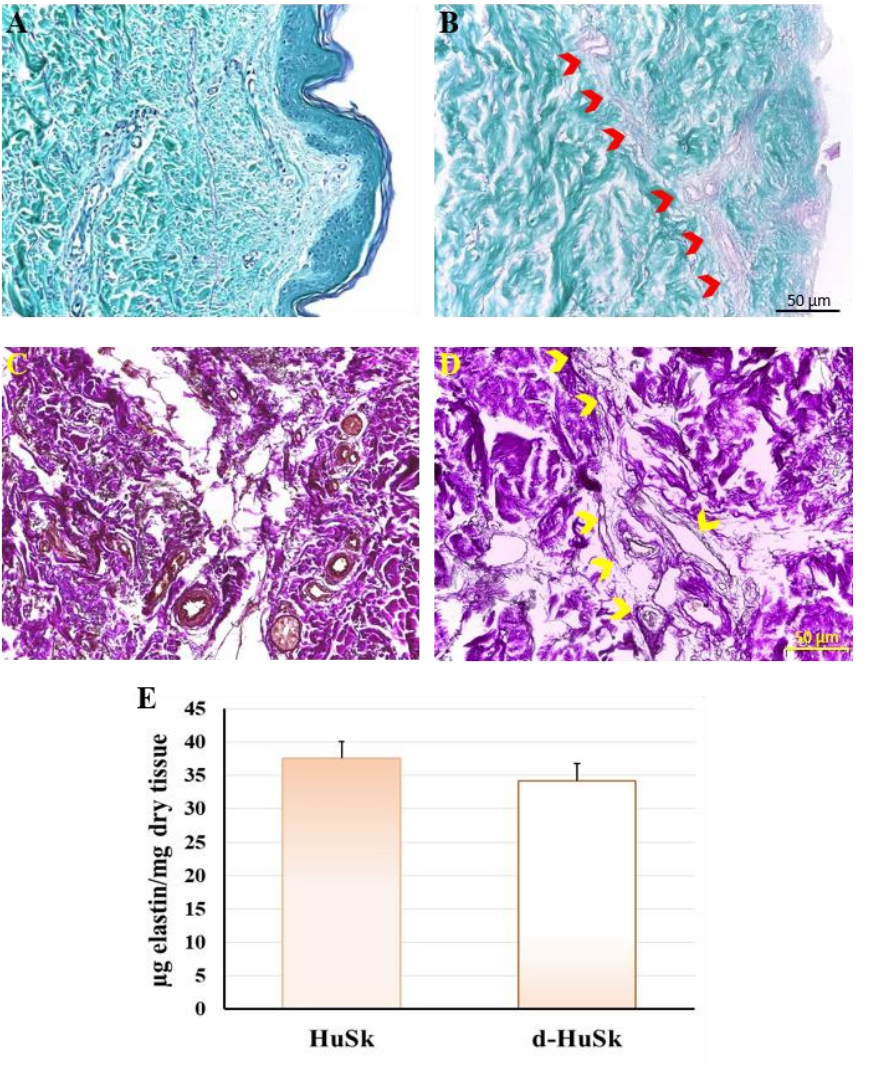

Figure 9. Histochemical and quantitative analysis of elastin content in native human skin (HuSK) and in d-HuSk. A-D: Representative images of the histochemical analysis performed by Paraldehyde fuchsin Gomori's (A, B) and Weigert Van Gieson (C, D) stainings showing the presence of elastic fibers in the dermis of native skin (A and C) and in d-HuSk (B and D). Patent blood vessels surrounded by abundant elastic fibers are apparent in d-HuSk (red and yellow arrowheads). (HuSk: native human skin). (Scale bar: 50 µm). E: Quantification of elastin showing comparable content of elastin in d-HuSk and native skin (HuSk). Data are expressed as mean ± SEM (n = 8).

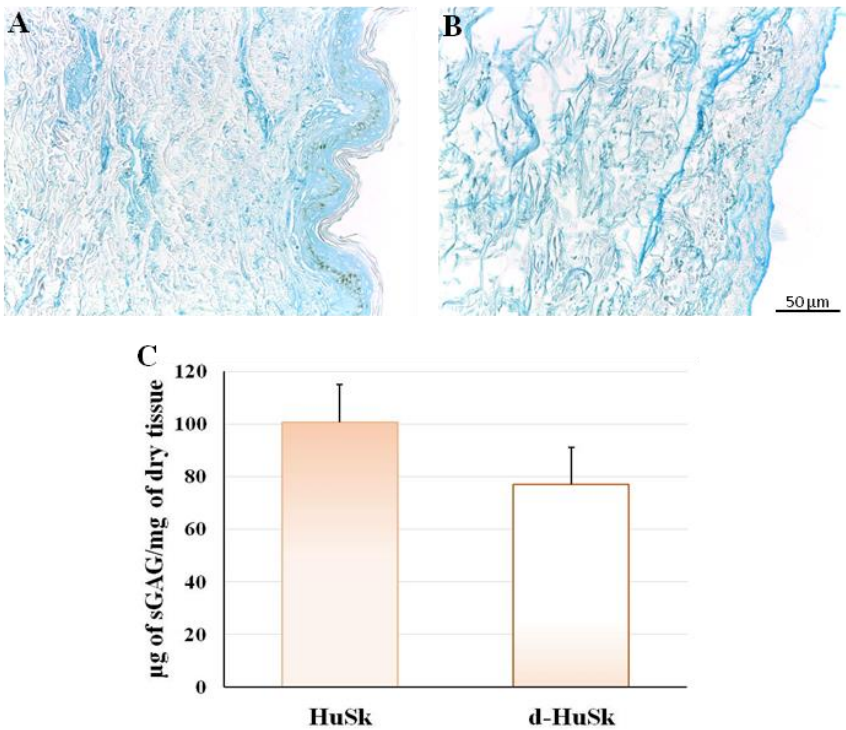

Figure 10. Histochemical and quantitative analysis of GAG content in native human skin (HuSK) and in d-HuSk. A and B: Representative images of the histochemical analysis performed by Alcian Blue staining and showing by the light blue color the presence of GAGs in the dermal connective tissue of native skin (A) and in d-HuSk (B). (Scale bar: 50 µm) C: Quantification of GAGs showing no statistically significant difference in content of GAGs in d-HuSk and native skin (HuSk). Data are expressed as mean ± SEM (n = 5).

Interestingly, due to the presence of elastin and GAGs d-HuSk holds the potential to deliver mechanical stimuli that support and promote cardiac differentiation (56, 80, 81).

Indeed, a close relationship between the differentiation of cardiac myocytes and the accumulation of elastin in embryoid bodies has been recently reported (82), along with the evidence that elastin content in the left ventricle of developing mammalian heart increases throughout the developmental stages but decreases soon after birth probably as a stimulus for complete maturation of cardiac myocytes (83).

Furthermore, the early tubular heart is formed by the endocardium and the myocardium with the interposed earliest form of cardiac ECM, the cardiac jelly. The cardiac jelly consists primarily of collagen, glycoproteins and GAGs (84). At this very early stage of cardiac development, by controlling cardiac jelly hydration, GAGs play a major role in exerting compressive strength on the myocardium that drives cardiac chamber expansion (85). Hence the higher content of GAGs in d-HuSk might be crucial for both conferring elasticity and driving cardiac differentiation. Such hypothesis is supported by both the evidence emerging from preliminary studies on mechanical characterization that the stiffness of d-HuSk, measured as the elastic modulus at increasing levels of strain by uniaxial tensile tests, closely matches the range of end diastolic values of human myocardium (86, 87) and the evidence that the lack of GAGs in mouse embryo leads to severe defects in cardiac chamber formation and loss of trabeculation (88).

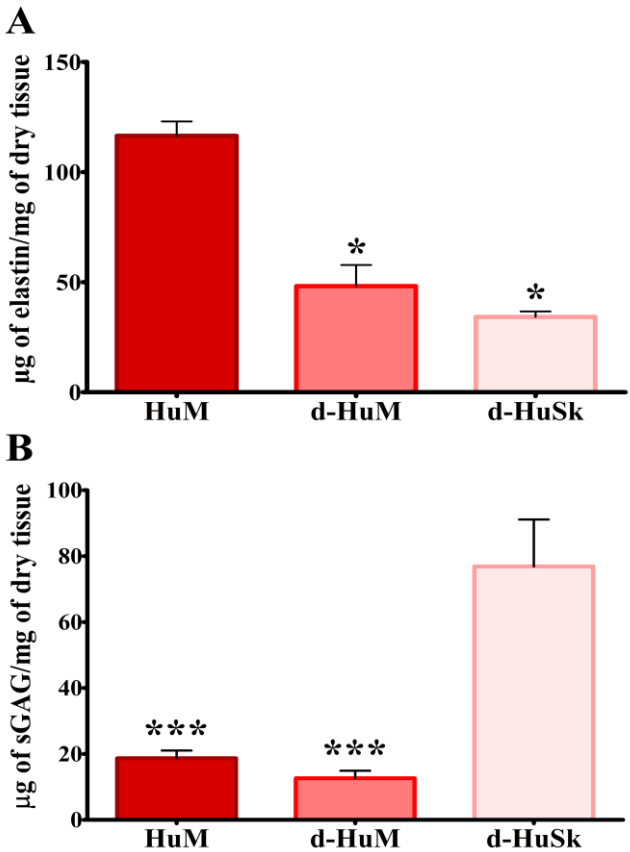

Figure 11. Comparative analysis of the content of elastin and GAGs in human myocardium and d-HuSk by quantitative dye-binding assays. A: Graphical representation of quantitative analysis of elastin content showing the presence of significantly higher content of elastin in native human myocardium (HuM) than in decellularized human myocardium (d-HuM) or in d-HuSK (n = 8). There is no statistically significant difference in the elastin content between d-HuM and d-HuSk, instead. B: graphical representation of quantitative analysis of GAG content showing significantly higher content of GAGs in d-HuSK. than in human myocardium, both native and decellularized (n = 5). There is no statistically significant difference in the GAG content between HuM and d-HuM. Data are expressed as mean ± SEM, asterisks are indicators of p value obtained as follows: significant (* $p \leq 0.05$) and extremely significant (*** $p \leq 0.001$).

3.4 The profile of growth factors of d-HuSk is comparable to that of the cardiac native matrix

Growth factors are signaling molecules known to regulate a plethora of tissue and cellular functions and their importance has been widely recognized also in tissue engineering (89). The ECM is known to function as a storage for growth factors (90) that are bound to ECM components like GAGs.

Therefore, we performed a comparative analysis of the growth factor profile of d-HuSk and d-HuM by protein array. Interestingly, the analysis revealed that d-HuSk contained, to a large extent, the same growth factors of the cardiac native matrix (Fig. 12, A-C). Indeed, both d-ECMs contained growth factors, like hepatocyte growth factor (HGF), insulin-like growth factor (IGF), stem cell factor (SCF), platelet-derived growth factor (PDGF) and vascular endothelial growth factor (VEGF), but d-HuSk resulted enriched with growth factors that were virtually absent in d-HuM, like granulocyte-macrophage colony-stimulating factor (GMCSF) and transforming growth factor (TGF-beta) and also contained significantly higher amount of growth factors like basic fibroblast growth factor (bFGF) and epidermal growth factor (EGF) (Fig. 12, D).

These factors have been reported to be involved in a variety of cardiac processes. Particularly, HGF in the developing heart, influences cardiomyocyte proliferation and differentiation, while in the adult heart controls heart homeostasis, prevents oxidative stress in normal cardiomyocytes (91) and is thought to act as a modulator of cardiac repair (92). Additionally, the ligand-receptor systems HGF/Met has been extensively investigated for its role in cardiac regeneration and evidence supports its involvement in boosting migration, engraftment and commitment of cardiac stem cells (93) and in regulating MSC proliferation and differentiation into cardiac myocytes (94).

Similarly, PDGF and VEGF, other than playing a pivotal role in promoting and controlling angiogenesis and

neovascularization, have been reported to enhance the proliferation of MSCs and their differentiation into cardiac myocytes (94-96).

SCF is a growth factor abundantly expressed in the normal heart and for its ability to mobilize stem cells from the bone marrow is an interesting factor for stem cell-mediated cardiac repair. A role in controlling and attenuating cardiac remodeling has also been proposed for this growth factor (97).

An intriguing relationship between IGF-1 and cardiac myocytes has emerged from several studies, as IGF-1 has been shown to control differentiation, transcription, protein synthesis, and cell death of cardiac myocytes (98, 99). Further, IGF have cardioprotective functions mediated by the inhibition of cardiomyocytes apoptosis (100) and stimulates cardiac muscle regeneration mediated by the myocardial adult stem cells (101).

As mentioned above, d-HuSk contained significantly higher amount of bFGF, EGF, GM-CSF and TGF-beta. These factors are also involved in processes like cardiac stem cell migration and proliferation (102), cardioblast specification (103), cardiac development (104) mobilization and proliferation of endothelial progenitor cells (105), cardioprotection (106).

The abundance of growth factors in d-HuSk strengthens its suitability as a promising tool for cardiac tissue engineering. Noteworthily, considering the already described similarities between d-HuSk and the native cardiac matrix, d-HuSk might alone provide two of the three pillars of tissue engineering (Fig. 5), namely the scaffold and the signals, and then be exploited as stand-alone scaffold to boost cardiac regeneration by recruiting resident cardiac progenitor cells, or as a cellularized scaffold by preparing a cardiac engineered tissue *in vitro* with the cell population of choice.

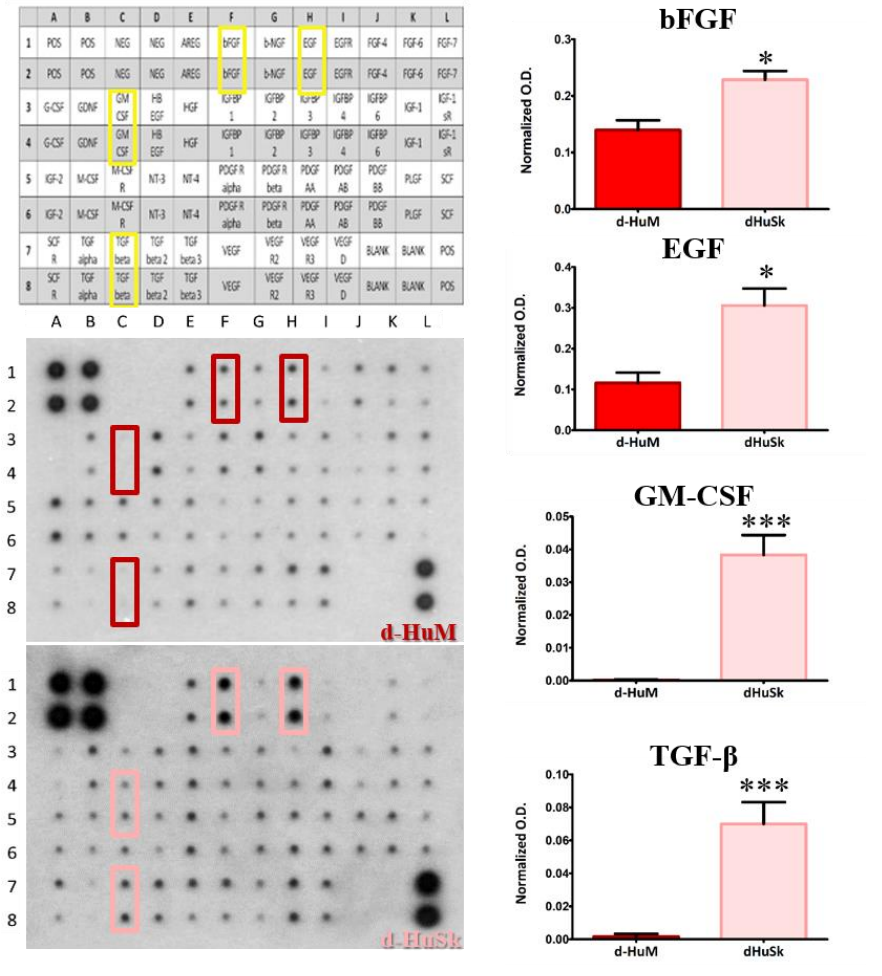

Figura 12. Analysis and quantification of growth factors evaluated by specific protein array. The representative images of membrane array (on the left) show that most of the 41 targets were present both in d-HuSk and d-HuM. However, it is immediately apparent a higher content of bFGF, EGF, GM-CSF and TGF-beta in d-HuSk, as shown by the reference array map in the upper left corner. The quantification of the aforementioned factors (on the right) shows their significantly higher content in d-HuSk. Each value expresses the mean ± SEM (n = 4). Asterisks were used to report significance in each comparison as follows: significant (* $p < 0.05$), very significant (*** $p < 0.001$). O.D.: optical density.

3.5 d-HuSk is a suitable environment for the engraftment and survival of human Cardiac Progenitor Cells (hCPCs)

In order to be considered suitable for regenerative medicine purposes, any scaffold must meet some key requirements with biocompatibility being one of them (52). This implies that the scaffold must have the ability to attract cells and sustain or promote their adhesion and survival exactly like the naturally occurring tissue microenvironment.

Thus, to evaluate the ability of d-HuSk to serve as a viable microenvironment capable of supporting hCPC homing, engraftment and survival, we seeded and cultured hCPCs on 600-μm-thick sections of d-HuSk and cultured them for up to four weeks. Additionally, to evaluate the effects of d-HuSk on hCPCs survival as compared to those of the cardiac native matrix, we seeded and cultured in the same conditions hCPCs on 600-μm-thick sections of d-HuM as a reference. Last, to assess whether d-HuSk had the potential to attract resident hCPCs and, then, to be used as a cell-free scaffold for cardiac tissue engineering, we subjected hCPCs seeded and cultured on d-HuM for four weeks to d-HuSk, by placing d-HuSk scaffolds in culture in the close proximity of recellularized d-HuM scaffolds.

Then, we analyzed by time-lapse microscopy the migration of hCPC from d-HuM to d-HuSk, while by the fluorescent staining with DAPI and SEM analysis we evaluated the engraftment of hCPCs on d-HuSk. Finally, by trypan blue exclusion assay we assessed the cell death rate and cell viability of hCPCs cultured on d-HuSK and on d-HuM, calculating the mean percentages of dead and alive cells over total cells at each timepoint considered.

The time-lapse movie obtained at a phase contrast microscope, showed the hCPCs migrating from d-HuM towards d-HuSk. Cells reached d-HuSk within a time ranging between 90 and 116 hours (Fig. 13).

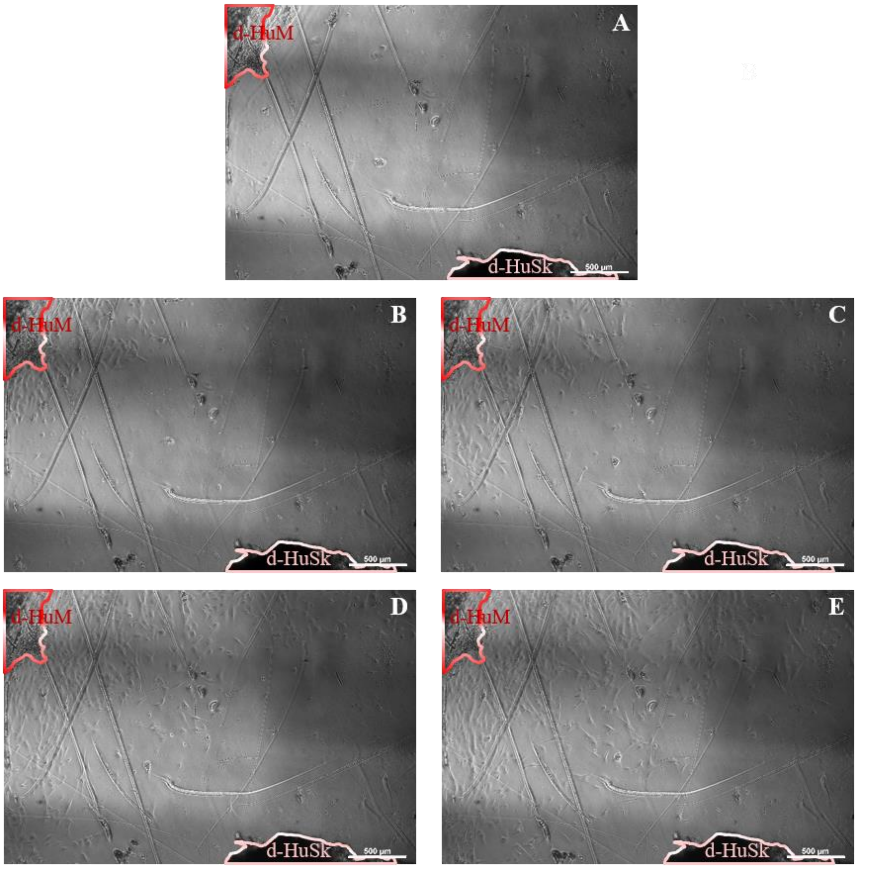

Figure 13. Migration of hCPCs from d-HuM to d-HuSk. Representative images at phase contrast microscope showing hCPCs engrated onto d-HuM migrating towards d-HuSk at different timepoints. A: time 0, B: after 24 hours, C: after 48 hours, D: after 72 hours, and E: after 96 hours. Cells reached d-HuSk within 90-116 hours. (Scale bar: 100 µm).

By binding the nuclear DNA the DAPI staining showed the presence of hCPCs that engrafted onto d-HuSk either after direct seeding or after having migrated *in vitro* to d-HuSk from d-HuM (Fig. 14).

SEM analysis not only confirmed the engraftment of hCPC on d-HuSk but allowed also to examine the morphology of hCPCs, that appeared either as mesenchymal-like cells characterized by elongated irregular shape and multiple filopodia or as rectangular/polygonal-shaped cells. Further, cell-to-cell contacts were apparent in some microscopic fields (Fig. 15).

48 hours after seeding the death rate of hCPCs seeded on the d-HuM or on d-HuSk did not differ significantly (9.814 ± 1.792% and 9.112 ± 1.532%, respectively) and on both matrices the death rate of hCPC decreased remarkably and progressively with time (3.402 ± 0.681% on d-HuM and 3.035 ± 0.529% on d-HuSK after 72 hours, 2.348 ± 0.779% on d-HuM and 1.857 ± 0.771% on d-HuSK after 96 hours, 1.2723 ± 0.678% on d-HuM and 1.190 ± 0.659% on d-HuSK after 120 hours, 0.750 ± 0.303% on d-HuM and 0.688 ± 0.239% on d-HuSK after 144 hours) till it reached values well below 1% of total cells, without any statistically significant differences between the two matrices (0.257 ± 0.107 % on d-HuM and 0.253 ± 0.104% on d-HuSk). Obviously, cell viability showed an inverted trend and increased with time on both d-HuM and d-HuSk. Specifically, the mean percentage of alive cells resulted 90.186 ± 1.792% and 90.888 ± 1.792% after 48 hours on d-HuM and d-HuSk, respectively, but then increased up to 99.743 ± 0.107% and 99.747 ± 0.107% after 7 days on d-HuM and d-HuSk, respectively (Fig. 16).

Based on the evidence emerging from the *in vitro* assessment of biocompatibility, d-HuSk environment was as safe as the native cardiac environment as demonstrated by the effects exerted by d-HuSk on migration, engraftment and survival of hCPCs. Moreover, being capable of attracting hCPCs engrafted onto cardiac native matrix and of supporting their engraftment, d-

HuSk holds great promise as a stand-alone scaffold for cardiac tissue engineering applications.

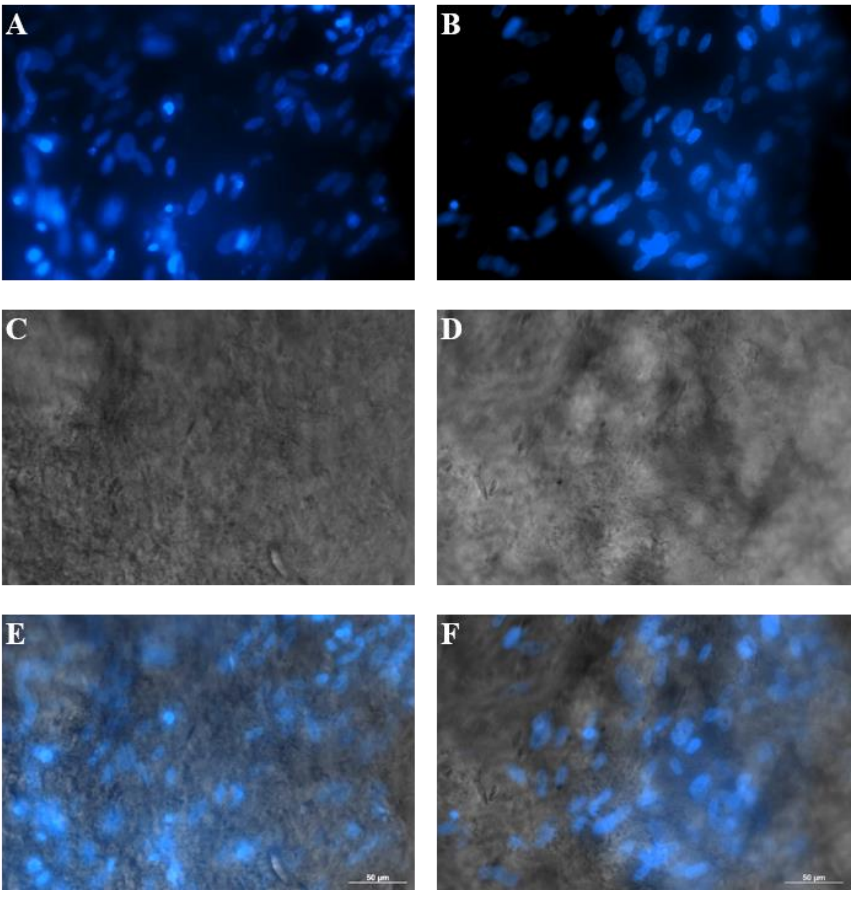

Figure 14. Fluorescent staining with DAPI of hCPCs engrafted on d-HuSk. Representative images showing by the nuclear staining with DAPI and the phase contrast microscope the presence of hCPCs engrated onto d-HuSk either after direct seeding (A, C, E) or after having migrated to d-HuSk from d-HuM (B, D, F). The merged pictures clearly show the distribution of hCPCs in d-HuSk. (Scale bar: 50 µm).

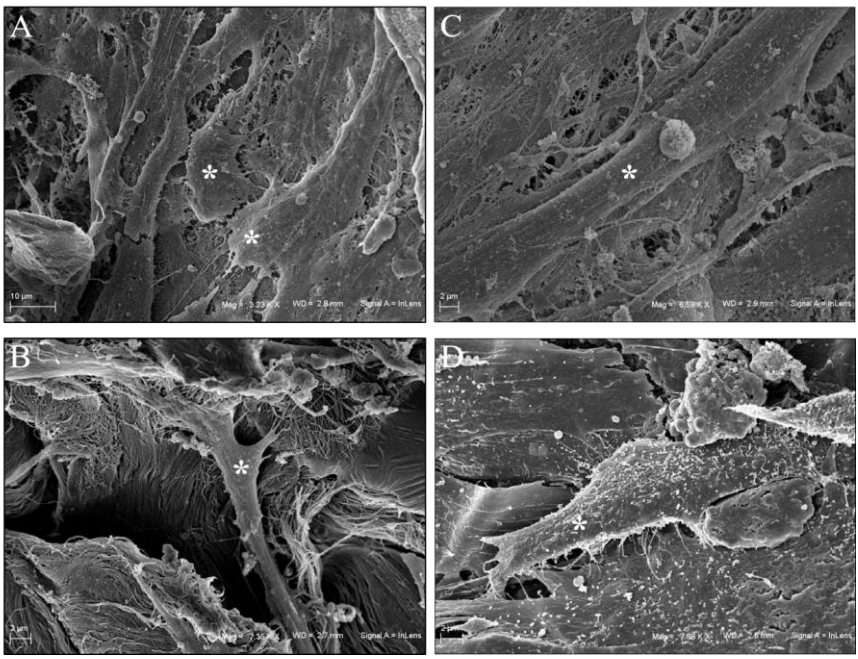

Fig. 15: SEM analysis of hCPCs engrafted onto d-HuSk. Representative images of SEM analysis of hCPC cultured on d-HuSk. White asterisks indicate the cells. In (A) two cells clearly spread onto d-HuSk that contact each other are shown. In (B) one cell with elongated irregular shape characterized by multiple filopodia is shown. This morphology is compatible with mesenchymal-like or mesenchymal derived cell. In C and D cells with an elongated rectangular/poligonal shape compatible with differentiating cardiomyocytes are shown. (Scale bar: 10 µm for A and 2 µm for B, C and D).

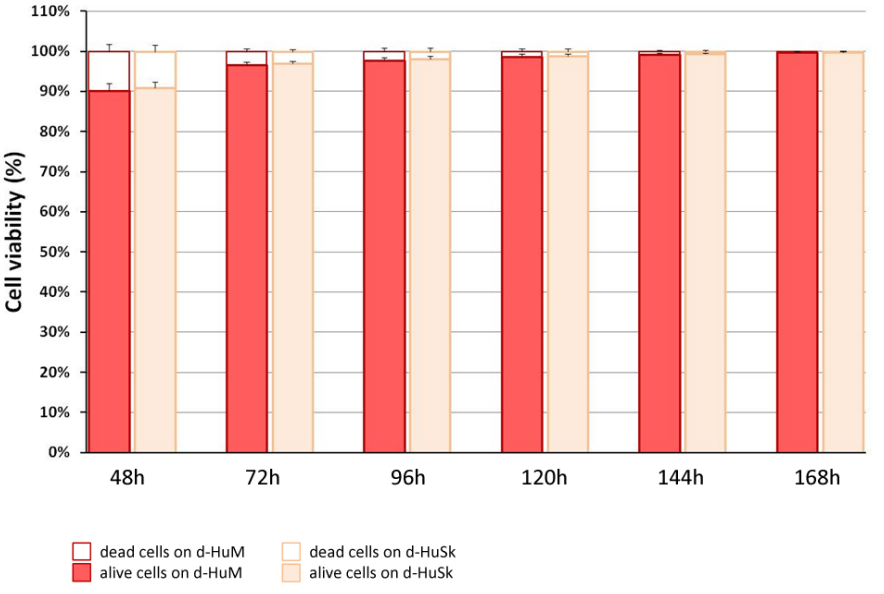

Figure 16. Quantification of cell death rate and viability of hCPCs on d-HuSk and d-HuM. Mean death rate and mean viability of hCPC cultured on d-HuSk or d-HuM, as measured by trypan blue exclusion assay. Cells were detached and assayed every day started at day 2 to allow them to attach. Then based on the ability of healthy cells to exclude the dye, dead cells were recognized by the blue staining with trypan blue and, hence, at any given timepoint the number of alive and death cells was obtained, averaged and calculated as the mean percentage ± SEM (n = 4). With time cell death rate dramatically decreased from around 9% to less than 1%, without any statistically significant differences between cells cultured on d-HuM or d-HuSk.

3.6 hCPCs retain on d-HuSk the potential to differentiate towards cardiac myocytes *in vitro*

Evidence collected thus far supported the hypothesis that d-HuSk might constitute a myocardial-like matrix. Loaded with signals that direct and control cardiac development and the homeostasis of the adult heart, d-HuSk could also be capable of supporting and promoting the differentiation of hCPCs into cardiac myocytes.

Hence, to assess the suitability of d-HuSk to serve as a cardiogenic environment for hCPCs, we analyzed the expression of genes specific for cardiac program (GATA4, TBX5) and for cardiac myocytes (CX43, CX37, TBX3, TBX5, MEF2C, ACTC1, MYH7) in hCPCs cultured on d-HuSk for four weeks by real-time PCR. To gain better insight into the possible effects of d-HuSk on hCPC expression of cardiac myocyte differentiation markers, we used as a reference the expression of the same markers in hCPC cultured in the same conditions on d-HuM.

Interestingly, from gene expression analysis emerged that the transcription of all cardiac specific genes investigated, either typical of early or late stages of differentiation, was significantly upregulated ($p \leq 0.05$) up to two-fold in hCPCs cultured on d-HuSk for 4 weeks (Fig. 17).

Additionally, to confirm the results of gene expression analysis, we evaluated at the protein level the expression of the cardiac myocyte markers Nkx 2.5, alpha-sarcomeric actin, connexin-43, desmin and dystrophin in hCPC cultured on d-HuSk for 4 weeks, by immunofluorescence.

The immunocytochemical analysis showed the immunopositivity in hCPC engrafted onto d-HuSk for the markers investigated. Clearly, the main cell population of CPC consisted of cells expressing Nkx 2.5 and alpha-sarcomeric actin (Fig. 18), as well as desmin, dystrophin and connexin-43 (Fig. 19) that are all markers specific for cardiac myocytes. Moreover, the alignment of actin filaments is suggestive of striated muscle. even though further investigation is needed to demonstrate the electrical coupling of the connexin-43 expressing cells in order to demonstrate their effective ability to form functional syncytia.

Although, based on previously discussed evidence, the expression of markers specific for cardiac myocytes by hCPCs engrafted onto d-HuSk was predictable, it is yet astounding that hCPCs expressed both at gene and protein level markers specific for cardiac myocytes on decellularized dermal matrix. Even more intriguing is the upregulation of gene transcription for such

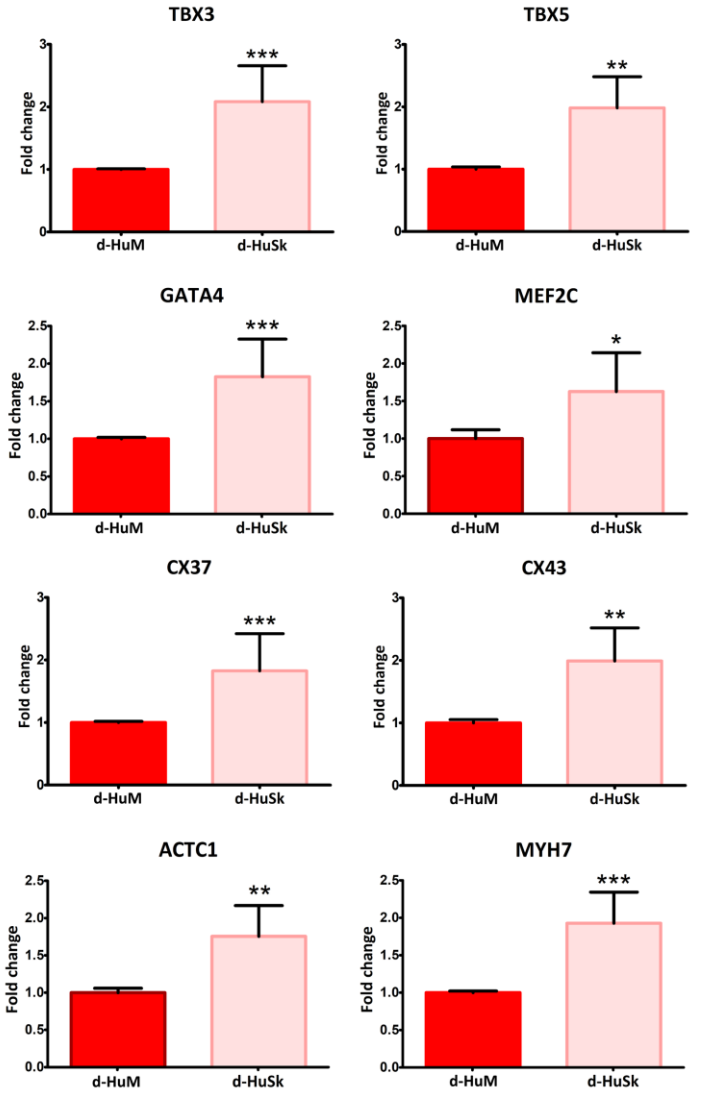

Figure 17. Analysis of gene expression of cardiac myocyte markers. Real-time PCR analysis of the expression of genes characteristic of cardiac myocytes showing an upregulation of the transcription for all markers in hCPCs cultured on d-HuSk when compared with hCPCs cultured on d-HuM. Data are expressed as mean ± SEM (n = 3). Asterisks are indicators of the p value obtained in each comparison as follows: significant (* $p \leq 0.05$), very significant (** $p < 0.001$ and extremely significant (*** $p \leq 0.001$).

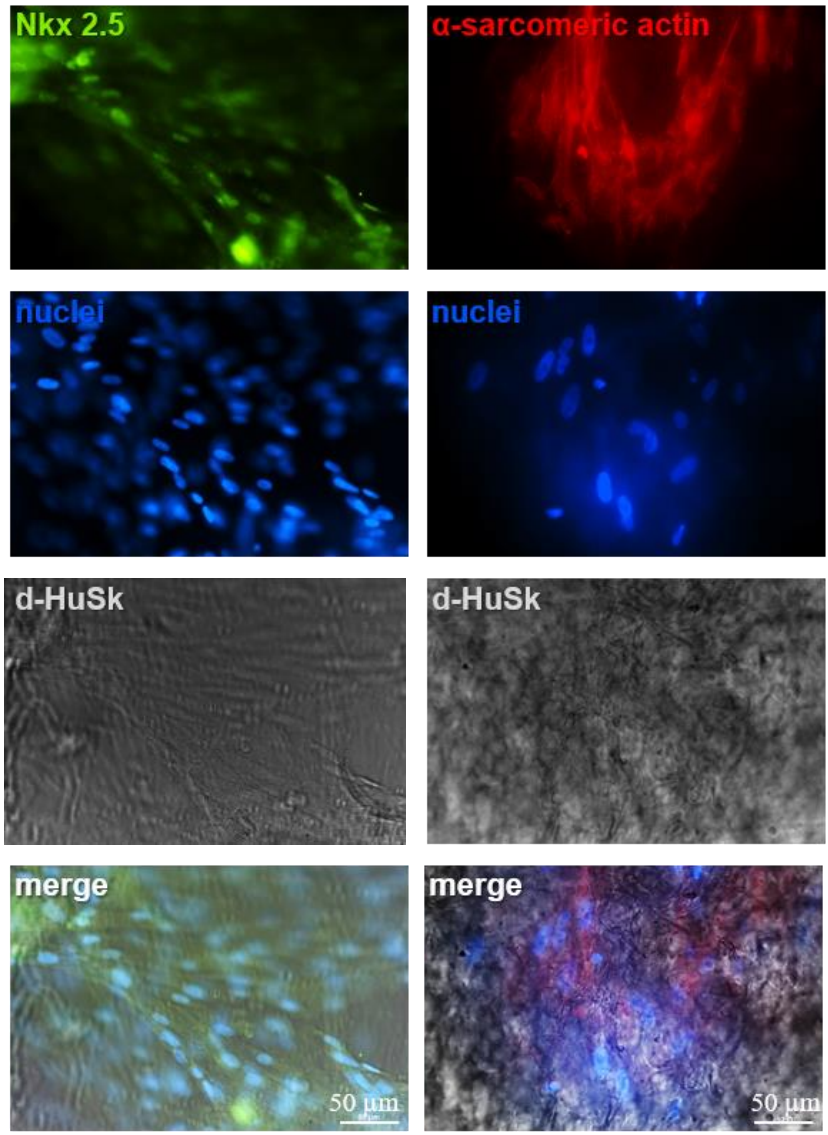

Fig. 18: Fluorescence microscopy analysis of hCPC cultured on d-HuSk for four weeks. Representative images of immunocytochemistry, showing the immunopositivity and distribution of Nkx 2.5 and alpha-sarcomeric actin in hCPC cultured on d-HuSk. (Scale bar: 5

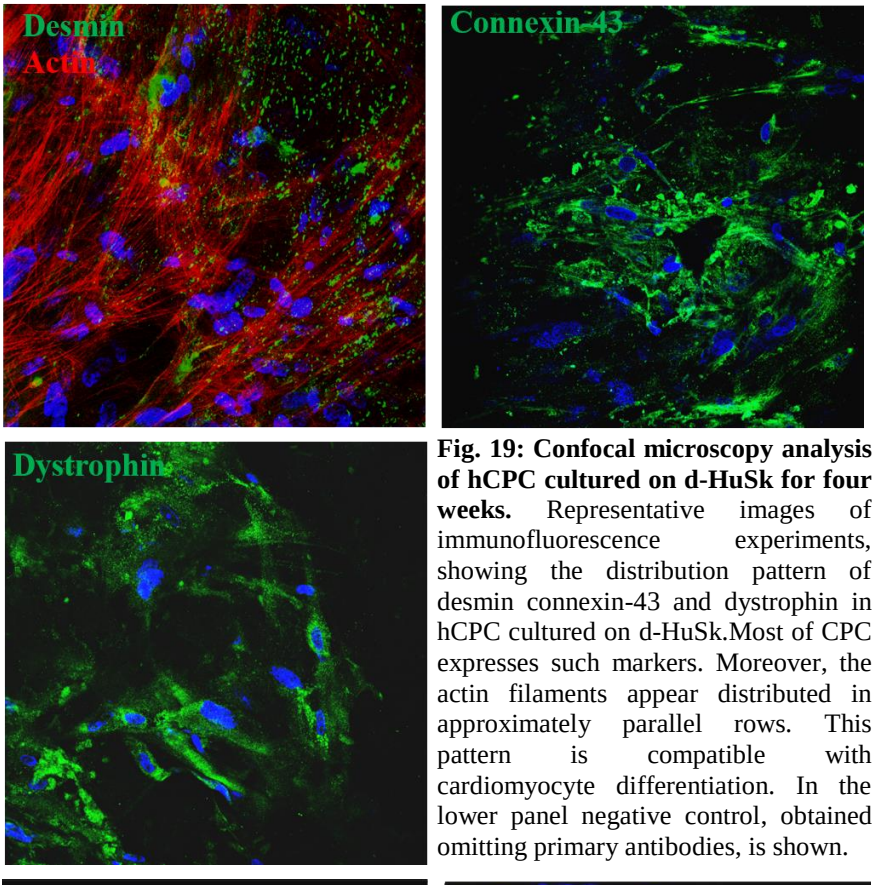

Fig. 19: Confocal microscopy analysis of hCPC cultured on d-HuSk for four weeks. Representative images of immunofluorescence experiments, showing the distribution pattern of desmin connexin-43 and dystrophin in hCPC cultured on d-HuSk.Most of CPC expresses such markers. Moreover, the actin filaments appear distributed in approximately parallel rows. This pattern is compatible with cardiomyocyte differentiation. In the lower panel negative control, obtained omitting primary antibodies, is shown.

markers, which, along with the morphology of cells observed at the SEM, supports the hypothesis that the decellularized human skin makes a myocardial-like environment that attracts resident CPCs, ensures their survival and sustains their differentiation.

4 Conclusions

In the scenario of an urgent need for more effective therapy of ischemic heart disease, tissue engineering has emerged as the only therapeutic approach that holds the potential to reestablish the structural, biomechanical and functional integrity of ischemic myocardium. However, the search for the best-performing and cost-effective scaffold capable of recapitulating biological and mechanical cues of cardiac microenvironment is still a primary goal of cardiac regenerative medicine.

With the present work we developed and evaluated *in vitro* a biological tool for cardiac regeneration that holds the potential to become a powerful alternative for both native matrix and synthetic scaffold.

d-HuSk fulfills the key requirements needed for a scaffold to warrant its use in tissue engineering. The biological nature of d-HuSk ensures a full biodegradability and, indeed, d-HuSk should be considered a temporary implant providing support to resident cells until its complete replacement by native tissue, as resident cells are expected to degrade the ECM and produce their own. Furthermore, the dermal ECM provides both sites of attachment for cell adhesion and a vascular network critical to ensure diffusion of nutrients, and, then, addresses two serious problems related to synthetic biomaterials.

However, the groundbreaking features of d-HuSk are its autologous origin and ability to support, *in vitro*, the engraftment, proliferation and differentiation potential of resident human cardiac progenitor cells (hCPCs). In fact, using d-HuSk as an autograft would imply transplanting a fully compatible scaffold capable of averting the immunological response and the risk of rejection that affect the heterologous and xenogeneic transplant or implant. Additionally, despite the different anatomical site of origin d-HuSk proved to be a suitable environment for hCPC, at least as cozy as the native one. If proven *in vivo*, such evidence has a tremendous potential, as d-HuSK might be used as an autologous and stand-

alone scaffold that promotes and sustains cardiac regeneration by resident hCPCs. Noticeably yet, as adult fibroblasts have been recently successfully reprogrammed to cardiac mature cells (107), the preparation of scaffolds of decellularized dermal ECM holds great promise to eventually evolve into the development of a complex therapeutic approach that offers, with one single intervention of skin harvesting, the possibility of constructing an engineered – fully autologous – myocardium using cardiac direct reprogramming of fibroblast to restore the cellular compartment and the decellularized dermal ECM to replace the extracellular compartment.

5 Limitations of the study

In this study we mainly focused on the effects of d-HuSk on CPCs, however further investigation is needed to provide more extensive insights on cell-matrix cross-talk and, specifically, to analyze whether and at to what extent CPCs can modify the composition of d-HuSk and adapt it to their requirements. This should include elucidating whether CPCs are capable to remodel and to convert d-HuSk from a fetal-like cardiac matrix to a mature cardiac matrix.

The native ECM influences cell behavior by its biological, chemical, physical and mechanical properties. Thus, a mechanical characterization at the macro and the micro scale should be performed to gain better knowledge of the signaling that are possibly delivered by d-HuSk and that might influence cell viability, proliferation, migration and differentiation.

Although the evidence that CPCs retain their ability to differentiate on biological scaffold obtained from different and more easily accessible ECM represents an important advance in cardiovascular regenerative medicine, as it overcomes problems related to the preparation of myocardial biological scaffolds, such evidence emerges from an *in vitro* study. Undoubtedly, *in vivo* studies designed to understand also mechanical properties, should advance its clinical utility.

6 Materials and methods

6.1 Tissue specimens

Skin specimens were collected from patients undergoing abdominoplasty (n = 8, mean age 42.25 ± 7.94 years). Upon receipt, specimens were washed in physiological saline, then subcutaneous fat tissue was removed, and multiple samples were cut. Resulting samples were then promptly processed for histological analysis, decellularization, or snap frozen until use. Cardiac specimens were harvested from macroscopically uninjured areas of the free wall of the left ventricle of hearts of cardiac transplant recipients (n = 10, mean age 49.5 ± 4,7 years). Specimens were washed in physiological saline and then cut into multiple samples that were processed for decellularization, or enzymatically digested to isolate hCPCs, or snap-frozen until use. Patients provided written informed consent and specimens were collected without patient identifiers, following protocols approved by the hospital and in conformity with the principles outlined in the Declaration of Helsinki.

6.2 Decellularization of human skin

Human Skin (HuSk) specimens were cut into smaller samples (2 x 1 cm, length by width) and incubated in decellularizing solution containing 1% SDS (w/v) and 1% Triton (v/v), for 24 hours under constant stirring. The solution was replaced every 8 hours. During the procedure the epidermis detached from the dermis and was removed. Samples were then rinsed for 24 hours in antibiotic solution containing 0.25 μg/ml Amphotericin B, 100 U/ml Penicillin, 50 U/ml Streptomycin in PBS, and then for an additional 30 minutes in sterile bidistilled water. After decellularization, samples of d-HuSk were either fixed in formalin for paraffin embedding and histological analysis or stored at -80°C until use for decellularization and molecular analysis.

6.3 Decellularization of human myocardium

Following a recently published protocol (60), frozen samples of human myocardium were mounted on a cryostat chuck using Tissue Freezing Medium (Leica Microsystems, Wetzlar, Germany) and cut into 600-µm-thick sections by a Leica CM1950 cryostat (Leica Microsystems). Cryosections were collected into sterile 50-ml sterile plastic tubes and then incubated for 24 hours in decellularizing solution containing 1% SDS (w/v) and 1% Triton (v/v). Cryosections were decellularized under constant agitation on an orbital shaker. The decellularizing solution was replaced every 8 hours. Sections were then rinsed for 24 hours in antibiotic solution containing 0.25 µg/ml Amphotericin B, 100 U/ml Penicillin, 50 U/ml Streptomycin in PBS, and then for an additional 30 minutes in sterile bidistilled water. After decellularization, sections of d-HuM were either stored at 4°C in sterile bidistilled water or at -80°C until use for comparative analysis of d-HuSk and d-HuM.

6.4 Quantitative measurement of DNA content

Genomic DNA was extracted from frozen native (n = 4) and decellularized human skin (n = 6), using the AllPrep DNA/RNA Mini Kit (Qiagen, Hilden, Germany), according to the manufacturer's instructions. Briefly, tissue samples were lysed and homogenized in a highly denaturing buffer containing guanidine-isothiocyanate. The buffer ensured isolation of intact DNA and RNA by inactivating DNases and RNases. Then the passage of lysates through an AllPrep DNA spin column allowed selective and efficient binding of genomic DNA. The columns were washed and pure, ready-to-use, DNA was then eluted. DNA concentration was determined by measuring the absorbance at 260 nm using a Nanodrop1000 (Thermo Scientific, Waltham, MA, USA) and the gDNA band was visualized with agarose electrophoresis. Data were averaged and expressed as the mean ng of DNA ± SE per mg of dry tissue.

6.5 Histochemistry

Specimens of native skin (n = 8) and d-HuSk (n = 8) were fixed in 10% neutral-buffered formalin and then processed for paraffin embedding, following a routine procedure. Briefly, formalin-fixed samples were dehydrated in an ascending series of alcohols, infiltrated with liquid paraffin and then embedded in paraffin in molds. Paraffin blocks were then sliced into serial 5-µm-thick sections that were mounted onto microscope slides. Following standard protocols, after deparaffinization and rehydration in a descending alcohol series, sections were stained with Fast H&E (Hematoxylin and Eosin) staining kit (Bio-Optica, Milan, Italy) to evaluate tissue architecture and effectiveness of decellularization, with Paraldehyde Fuchsin Gomori's Method and Weigert - Van Gieson Quick Method staining kits (Bio-Optica) to detect elastic fibers and with Alcian Blue pH 2,5 staining kit (Bio-Optica) to detect GAGs and Hyaluronic Acid. Stained sections were observed and evaluated by at least three independent observers using a light microscope DM2000 Led (Leica Microsystems) equipped with the ICC50HD camera (Leica Microsystems) for microphotography.

6.6 Immunohistochemistry

Paraffin sections of d-HuSk were prepared as described for histochemistry and immunostained using indirect immunoperoxidase technique to detect the presence and analyze the distribution of collagens, fibronectin, tenascin and laminin using specific antibodies. The presence and localization of antigen-antibody complexes were revealed by the UltraVision LP Detection System HRP Polymer & DAB Plus Chromogen (Thermo Scientific, Waltham, MA, USA), following the manufacturer's protocol. First, sections were incubated with UltraVision Hydrogen Peroxide Block to reduce non-specific background due to endogenous peroxidase. Next, sections were washed in PBS and incubated with Ultra Vision Protein Block, to reduce non-specific

bindings of antibodies. Then, slides were incubated with primary antibodies against human type I collagen, fibronectin, tenascin and laminin (all from Sigma-Aldrich, St. Louis, MO, USA). After further washes in PBS, sections were incubated with Primary Antibody Enhancer, and then with HRP Polymer. Finally, sections were incubated with DAB chromogen for the visualization of the polymer complex. Nuclei counterstaining with Mayer's hematoxylin (Bio-Optica, Milan, Italy), dehydration and coverglass mounting with Bio Mount mounting medium (Bio-Optica) were the last steps before analysis. All steps were performed at room temperature, except for the incubation with primary antibody that was performed at 37°C. Stained sections were evaluated and documented by at least three independent observers using a light microscope DM2000 Led (Leica Microsystems) equipped with an ICC50HD camera (Leica Microsystems).

6.7 Quantitative measurement of elastin

Elastin was extracted from samples of native skin (n = 8) weighting 20 mg each and from samples of d-HuSk (n = 8) and d-HuM (n = 8) weighting 20 mg each before decellularization. The extraction was performed by heating specimens at 100°C for three one-hour periods in 0.25M oxalic acid, in accordance with manufacturer's directions. Tissue extracts were then assayed in the Fastin Elastin Assay quantitative dye-binding method (Biocolor, Ltd, Carrickfergus, UK), following instructions provided by manufacturer. Briefly, samples were incubated with Elastin Precipitating Reagent to allow the precipitation of α-elastin. Dye Reagent was then added and the Elastin-Dye complexes that formed were exposed to the Dye Dissociation Reagent before proceeding with absorbance reading. All samples were tested in triplicate and the absorbance was read at 490 nm using the ELx800 Absorbance Microplate Reader (BioTek Instruments, Winooski, VT, USA), and analyzed with Microsoft Excel (Microsoft Corp, Redmond, WA, USA) to generate the calibration curve and calculate the final concentration of elastin for each absorbance

reading. Data were averaged and expressed as the mean amount of elastin (μg) ± SE per mg of wet tissue.

6.8 Quantitative measurement of GAG

As described for the Fastin Elastin Assay, samples of 20 mg each of native skin (n = 5) and samples of both d-HuSk (n = 5) and d-HuM (n = 5) weighting 20 mg each before decellularization were assayed for the quantitative analysis of sGAG content in Blyscan Assay (Biocolor, Ltd). All samples were tested in triplicate. Assay was performed according to instruction manual provided with the kit. Briefly, samples were digested by incubation with Papain Extraction Reagent at 65°C for 3 hours. Digested samples were then incubated with Blyscan Dye Reagent to allow the formation and precipitation of glycosaminoglycan-dye complex. The subsequent addition of the Dissociation Reagent to samples caused the release of s-Glycosaminoglycan-Bound dye whose absorbance was read at 600 nm using the BioPhotometer (Eppendorf) and analyzed with Microsoft Excel (Microsoft Corp, Redmond, WA, USA) to generate the calibration curve and calculate the final concentration of elastin for each absorbance reading. Data were averaged and expressed as the mean amount of sGAG (μg) ± SE per mg of wet tissue.

6.9 Growth Factor Array

d-HuSk and d-HuM samples were lysed in lysis buffer containing Tris-HCl, 5Mm EDTA, Triton-X100, 0.01M DTT, PMSF, and protease inhibitor cocktail. Protein concentration was quantified by a Bradford assay, and then 100 μg of each tissue lysate was assayed in the Human Growth Factor Array C1 (Raybiotech, Norcross, GA, USA). The assay allows the simultaneous detection of 41 targets. Following the assay protocol supplied with reagents, array membranes were blocked with blocking buffer for 30 minutes at room temperature, and then incubated with samples at room temperature for 2.5 hours.

Membranes were then washed in wash buffer I and in wash buffer II and incubated with biotin-conjugated antibody overnight at 4°C. Membranes were washed and incubated with horseradish peroxidase (HRP)-conjugated streptavidin for 2 hours at room temperature. One final wash was performed to remove unbound reagents. All array steps were carried out with agitation on an orbital shaker. Membranes were then developed with the detection buffer, exposed to film, and processed by autoradiography. For the analysis, arrays were scanned and spot signal densities from corresponding images were obtained using ImageJ densitometry software (https://imagej.nih.gov/ij/download.html). Final values were obtained by subtracting background from the densitometry data and normalizing toward the positive control signals. Data were expressed as the mean ± SEM.

6.10 hCPC isolation and culture

hCPCs were isolated from human cardiac specimens, as previously described (15). Briefly, myocardial specimens were dissected, minced, and enzymatically disaggregated by incubation in 0.25% trypsin (Sigma-Aldrich) for 6 hours at 4°C and in 0.1% (w/v) collagenase II (Sigma-Aldrich) for 30 minutes at 37°C. The digestion was stopped by adding double volume of HBSS (Sigma-Aldrich) supplemented with 10% FBS (Sigma-Aldrich). Resulting fragments of tissue were further disaggregated by pipetting. Tissue debris and cardiomyocytes were then removed by sequential centrifugation at 100 g for 2 minutes, passage through a 40-μm cell strainer (BD Biosciences, Franklin Lakes, NJ, USA) and centrifugation at 400 g for 5 minutes. Obtained cell population was then incubated with anti-fibroblast MicroBeads (Miltenyi Biotec, Bergisch Gladbach, Germany), to magnetically label fibroblasts that were removed loading cells onto a MACS column (Miltenyi Biotec) placed in the magnetic field of a MACS separator (Miltenyi Biotec), while unlabeled cells ran through the column. Hence, the negative fraction of hCPCs was collected and used to prepare 3D cultures with d-HuSk and d-HuM.

6.11 Preparation of d-ECM scaffolds for 3D cultures of hCPCs

As previously described for myocardium (60), frozen specimens of d-HuSk were mounted on a cryostat chuck using Tissue Freezing Medium (Leica Microsystems, Wetzlar, Germany), sliced into 600-µm-thick sections by a Leica CM1950 cryostat (Leica Microsystems) and collected in sterile cell culture dishes. 600-µm-thick cryosections of d-Husk and d-HuM were sterilized by exposure to ultraviolet radiation for 40 minutes and rehydrated for 7 days with F12K medium in an incubator at 37° C with 5% CO_2. d-HuSk and d-HuM sterilized and rehydrated cryosections were then stored in standard culture conditions with the same medium until their use as 3D scaffolds for the culture of hCPCs.

6.12 *In vitro* assessment of d-HuSk cytocompatibility

Sterilized and rehydrated 600-µm-thick cryosections of d-Husk (n = 4) and d-HuM (n = 4) were cut into smaller fragments to fit the wells of the culture plate. The fragments of d-HuSk and d-HuM were then placed into the wells of sterile 96-well culture plates, seeded with $5x10^4$ hCPCs and cultured with Ham's F12 medium (Sigma-Aldrich) supplemented with 10% FBS (Sigma-Aldrich), 5% horse serum (Sigma-Aldrich), 10 ng/ml basic fibroblast growth factor (bFGF) (Peprotech, Rocky Hill, NJ, USA), and 50 IU/ml penicillin G-streptomycin (Sigma-Aldrich) (F12K medium) in an incubator at 37° C with 5% CO_2. Cell were allowed to adhere to the matrices for 48 hours after seeding. Afterwards, cell death rate of hCPCs cultured onto d-Husk and d-HuM was assessed every 24 hours for one week, using trypan blue exclusion assay. Following a previously published protocol (60) every 24 hours cells were detached from subsets of wells in the multiwell plates by incubation with 0.25% trypsin-EDTA solution (Sigma-Aldrich) for 10 minutes. Trypsin was inactivated by adding culture medium and detached cells were collected and centrifuged at 400 g

for 5 minutes. Cells were then stained with trypan blue stain (0.4% in PBS) (Lonza, Walkersville, MD, USA) for 2 minutes at room temperature and counted using a hemocytometer. As previously described (60), the assay is based on the ability of alive cells to uptake and exclude the dye that allows to recognize them as unstained cells among the dead cells that are not capable of excluding the dye and stain blue. Thus, the assay allows the computation of both cell death rate and cell viability. The percentage of both dead and alive cells over total cells for each time point and both on d-HuSk and d-HuM was calculated and expressed as the mean percentages of the total number of cells ± SEM.

6.13 Assessment of ability of d-HuSk to support hCPC engraftment *in vitro*

$6.5x10^5$ hCPCs were seeded onto 600-µm-thick cryosections of d-HuM (n = 5) in sterile 35-mm culture dishes sterilized and rehydrated as described above. Cells were then cultured with F12K medium in an incubator at 37° C with 5% CO_2 for four weeks. Afterwards, cells adherent to the plastic dishes were scraped off with a cell scraper and sterilized and rehydrated 600-µm-thick cryosections of d-Husk were placed in culture near the d-HuM cryosections seeded with hCPCs. Culture dishes carrying both seeded d-HuM and unseeded d-HuSk were then cultured for four additional weeks with F12K medium at 37° C and in the presence of 5% CO_2 in a standard incubator or in a stage incubator mounted on a phase-contrast microscope. Additionally, $5x10^5$ hCPCs were seeded onto sterilized and rehydrated 600-µm-thick cryosections of d-Husk (n = 3) in sterile 35-mm culture dishes, and with F12K medium in an incubator at 37° C with 5% CO_2 for four weeks. Culture dishes were checked every day and medium was replaced every 3 days.

6.13.1 Live cell imaging analysis of repopulation of d-HuSk by hCPC residing on d-HuM

Culture dishes carrying both seeded d-HuM and unseeded d-HuSk were cultured with F12K medium at 37° C and in the presence of 5% CO_2 in a Stage Top Incubator (Okolab, Pozzuoli, Italy) mounted on a Nikon Eclipse Ti-E Microscope DS-Qi2 (Nikon, Tokyo, Japan) for the first week of culture to follow possible homing of CPCs from d-HuM to d-HuSk. Live cell imaging was employed to document the repopulation of d-HuSk by hCPCs residing onto d-HuM acquiring one picture every thirty minutes for 120 hours by digital camera (Nikon) and NIS Elements software (Nikon). After five days, d-HuSk sections cultured with d-HuM sections seeded with hCPCs were fixed in 4% paraformaldehyde for 20 minutes at room temperature, then stained with DAPI for 15 minutes at room temperature and analyzed by a Nikon Eclipse Ti-E Microscope DS-Qi2 (Nikon) to evaluate the presence of cells migrated from d-HuM to d-HuSk.

6.13.2 Scanning Electron microscopy analysis

Surface ultrastructure of d-Husk cryosections seeded with hCPCs was studied by Scanning Electron Microscopy (SEM). Briefly, samples fixed in 10% neutral-buffered formalin were dehydrated with ascending ethanol series (30 to 100%), subjected to Critical Point Dryer (EMITECH K850), mounted on a stub and sputtered with platinum-palladium Denton Vacuum (DESK V). FESEM (Field-Emission SEM) Supra 40 (ZEISS; EHT = 5.00 kV, WD = 22 mm, detector in lens) was used for observation.

6.14 Analysis of the effects of d-HuSk on hCPC myogenic differentiation potential *in vitro*

$5x10^5$ hCPCs were seeded onto 600-µm-thick cryosections of d-HuM (n = 6) and d-Husk (n = 6) in sterile 35-mm culture dishes sterilized and rehydrated as described before, and cultured

with F12K medium in an incubator at 37° C with 5% CO_2 for 4 weeks. Culture dishes were checked every day and medium was replaced every 3 days.

6.14.1 Gene expression analysis by Real-time PCR

Total RNA was extracted from hCPCs both migrated (6.13) and directly seeded onto d-HuSk (6.13 and 6.14) and cultured for four weeks, using Isol-RNA Lysis Reagent (5Prime, Hamburg, Germany) following the instructions provided by the manufacturer. Similarly, total RNA was extracted from hCPCs cultured on d-HuM (6.13 and 6.14) for four weeks, to serve as control. RNA was dissolved in RNase-free water, and the final concentration was determined using a Nanodrop 1000 spectrophotometer (Thermo Scientific, Waltham, MA, USA). All RNA samples were checked for quality and were considered suitable for gene expression profiling experiments. Then, 100 ng of RNA extracted from each sample was reverse transcribed into cDNA using a QuantiTect Reverse Transcription Kit (Qiagen). Expression of genes specific for cardiac myocytes (GATA4, ACTC1, MYH7, CX37, CX43, NKX2.5, MEF2C, TBX3 and TBX5) was quantified by real-time qPCR using 5Prime Hot MasterMix (5Prime) in Mastercycler ep realplex (Eppendorf). Detection was performed by the fluorescence dye SYBR Green I. All samples were tested in triplicate with the housekeeping gene (GAPDH) to correct for variations in RNA quality and quantity. Comparative quantification of target gene expression in the samples was performed based on the cycle threshold (Ct) normalized to the housekeeping gene.

6.14.2 Immunofluorescence

Immunofluorescence was performed on hCPCs cultured on d-HuSk for 4 weeks. Samples were fixed in 4% paraformaldehyde for 20 minutes at room temperature and then washed in PBS. To block non-specific binding from the donkey secondary antibody, samples were incubated with 10% donkey serum for 30 minutes at

room temperature and then, without washing, with the primary antibodies anti-actin (α-sarcomeric) (Sigma-Aldrich), Nkx 2.5, (Abcam, Cambridge, UK) for 1 hour at 37°C in a humified chamber. Sections were then washed in PBS and incubated with matching secondary antibodies conjugated with fluorescein or rhodamine (Jackson Immuno-Research Europe, Newmarket, UK) for 1 hour at 37°C. Nuclear counterstaining was performed by DAPI (Sigma-Aldrich) and sections were covered with a coverglass using the VECTASHIELD Antifade Mounting Medium (Vector Labs, Burlingame, CA, USA). Microscopic analysis and digital microphotography were performed by three independent researchers with a Nikon Eclipse Ti-E Microscope DS-Qi2 by NIS Elements software (Nikon Instruments, Tokyo, Japan). The expression of cardiac myocytes differentiation markers was also analyzed by confocal microscopy. Specifically, formalin-fixed samples were permeabilized for 3 hours with a permeabilizing solution containing 1% BSA and 0.1% Triton in PBS, then blocked with 5% donkey serum and incubated overnight with anti-desmin, anti connexin-43, or anti-dystrofin antibodies (Sigma-Aldrich). Then samples were extensively washed with PBS and incubated for 1 hour and 30 minutes with a fluorescein-conjugated donkey anti-mouse (Jackson Immuno-Research Europe). Rhodamin-conjugated phalloidin was used to detect actin cytoskeleton while TO-PRO3 iodide fluorescent dye 642/661 (Invitrogen) was used for nuclear staining. As a negative control, the primary antibody was omitted. Microscopic analysis was performed by a Leica Confocal Microscope (Laser Scanning TCS SP2 equipped with Kr/Ar and He/Ne lasers) performing optical spatial series with a step size of 2µm.

6.15 Statistical analysis

Statistical analysis was performed using GraphPad Prism 5.0 (GraphPad Software, La Jolla, CA, USA). Data obtained from the analysis of dsDNA content, the growth factor array, trypan blue exclusion assay and the Real-time PCR analysis were analyzed

using t test, while data obtained from the quantitative analysis of elastin and GAG content were analyzed using one-way analysis of variance (ANOVA) with Tukey-Kramer post-test. All experiments were performed in triplicate and all data were expressed as the mean ± SEM. A value of $p < 0.05$ was used to identify any statistically significant differences.

7 References

1. World Health Organization. Fact Sheets: Cardiovascular Diseases (CVDs). Available online: http://www.who.int/en/news-room/fact-sheets/detail/cardiovascular-diseases-(cvds).
2. World Health Organization. Fact Sheets: Noncommunicable Diseases (CVDs). Available online: http://www.who.int/en/news-room/fact-sheets/detail/noncommunicable-diseases.
3. Global Health Estimates 2016: Disease burden by Cause, Age, Sex, by Country and by Region, 2000-2016. Geneva, World Health Organization; 2018.
4. GBD 2015 Mortality and Causes of Death Collaborators. *Global, regional, and national life expectancy, all-cause mortality, and cause-specific mortality for 249 causes of death, 1980-2015: a systematic analysis for the Global Burden of Disease Study 2015*. Lancet. 2016, **388**(10053):1459-1544.
5. Patel, V., D. Chisholm., T. Dua, R. Laxminarayan, and M. E. Medina-Mora, editors. 2015. Mental, Neurological, and Substance Use Disorders. Disease Control Priorities, third edition, volume 4. Washington, DC: World Bank. doi:10.1596/978-1-4648-0426-7.
6. Caretto A, Lagattolla V. *Non-communicable diseases and adherence to Mediterranean diet*. Endocr Metab Immune Disord Drug Targets, 2015. **15**(1): 10-7.
7. Wahid A, Manek N, Nichols M, Kelly P, Foster C, Webster P, Kaur A, Friedemann, Smith C, Wilkins E, Rayner M, Roberts N, Scarborough P. *Quantifying the Association Between*

Physical Activity and Cardiovascular Disease and Diabetes: A Systematic Review and Meta-Analysis. J Am Heart Assoc, 2016. **5**(9)pii: e002495.

8. O'Keefe EL, Di Nicolantonio JJ, O' Keefe JH, Lavie CJ. *Alcohol and CV Health: Jekyll and Hyde J-Curves*. Prog Cardiovasc Dis, 2018. **61**(1): 68-75.
9. Danaei G, Ding EL, Mozaffarian D, et al. *The preventable causes of death in the United States: comparative risk assessment of dietary, lifestyle, and metabolic risk factors*. PLoS Med, 2009. **6**: e1000058.
10. Franco OH, Massaro JM, Civil J, Cobain MR, O'Malley B, D'Agostino RB Sr. *Trajectories of entering the metabolic syndrome: the framingham heart study*. Circulation, 2009. **120**(20): 1943-50.
11. Del Gobbo LC, Kalantarian S, Imamura F, Lemaitre R, Siscovick DS, Psaty BM, Mozaffarian D. *Contribution of Major Lifestyle Risk Factors for Incident Heart Failure in Older Adults: The Cardiovascular Health Study*. JACC Heart Fail, 2015. **3**(7): 520-528.
12. Li K, Monni S, Hüsing A, Wendt A, Kneisel J, Groß ML, Kaaks R. *Primary preventive potential of major lifestyle risk factors for acute myocardial infarction in men: an analysis of the EPIC-Heidelberg cohort*. Eur J Epidemiol, 2014. **29**(1): 27-34.
13. Nascimento BR, Brant LCC, Moraes DN, et al. *Global Health and cardiovascular disease*. Heart, 2014. **100**: 1743-1749.

14. Barbaresko J, Rienks J, Nöthlings U. *Lifestyle Indices and Cardiovascular Disease Risk: A Meta-analysis*. Am J Prev Med, 2018. **55**(4): 555-564.

15. World Health Organization. Noncommunicable Diseases Progress Monitor 2017. Available online: http://www.who.int/nmh/publications/ncd-progress-monitor-2015/en/.

16. Nichols M, Townsend N, Scarborough P, Rayner M. *Cardiovascular disease in Europe 2014: epidemiological update*. Eur Heart J, 2014. **35**(42): 2929.

17. Sanchis-Gomar F, Perez-Quilis C, Leischik R, Lucia A. *Epidemiology of coronary heart disease and acute coronary syndrome*. Ann Transl Med, 2016. **4**(13): 256.

18. Baggett TP, Liauw SS, Hwang SW. *Cardiovascular Disease and Homelessness*. J Am Coll Cardiol, 2018. **71**(22): 2585-2597.

19. Noncommunicable Diseases Progress Monitor, 2017. Geneva: World Health Organization; 2017. Licence: CC BY-NC-SA 3.0 IGO.

20. Ross R. *Atherosclerosis--an inflammatory disease*. N Engl J Med, 1999. **340**(2): 115-26.

21. Chan JK, Roth J, Oppenheim JJ, Tracey KJ, Vogl T, Feldmann M, Horwood N, Nanchahal J. *Alarmins: awaiting a clinical response*. J Clin Invest, 2012. **122**(8): 2711-9.

22. Frangogiannis NG. *The inflammatory response in myocardial injury, repair, and remodelling*. Nat Rev Cardiol, 2014. **11**(5): 255-65.

23. Dadson K, Kovacevic V, Sweeney G. *Mechanisms of Cardiac Fibrosis and Heart Failure*. In: Ian M.C. Dixon, Jeffrey T. Wigle (Eds.), Cardiac Fibrosis and Heart Failure: Cause or Effect?, 279-297, 2015.

24. Frangogiannis NG. *Matricellular proteins in cardiac adaptation and disease*. Physiol Rev, 2012. **92**(2): 635-88.

25. Sutton MG, Sharpe N. *Left ventricular remodeling after myocardial infarction: pathophysiology and therapy*. Circulation, 2000. **101**(25): 2981-8.

26. McKay RG, Pfeffer MA, Pasternak RC, Markis JE, Come PC, Nakao S, Alderman JD, Ferguson JJ, Safian RD, Grossman W. *Left ventricular remodeling after myocardial infarction: a corollary to infarct expansion*. Circulation, 1986. **74**(4): 693-702.

27. Pfeffer MA, Braunwald E. *Ventricular remodeling after myocardial infarction. Experimental observations and clinical implications*. Circulation, 1990. **81**(4): 1161-72.

28. Talman V, Ruskoaho H. *Cardiac fibrosis in myocardial infarction-from repair and remodeling to regeneration*. Cell Tissue Res, 2016. **365**(3): 563-81.

29. Weber, K. T., Sun, Y., Bhattacharya, S. K., Ahokas, R. A., & Gerling, I. C. *Myofibroblast-mediated mechanisms of pathological remodelling of the heart*. Nat Rev Cardiol, 2012. **10**(1): 15-26.

30. Leonard BL, Smaill BH, LeGrice IJ. *Structural remodeling and mechanical function in heart failure.* Microsc Microanal, 2012. **18**(1): 50-67.

31. Yancy CW, Jessup M, Bozkurt B, Butler J, Casey Jr DE, Colvin MM, DraznerMH, Filippatos G, Fonarow GC, Givertz MM, Hollenberg SM, Lindenfeld J, Masoudi FA, McBride PE, Peterson PN, Stevenson LW, Westlake C. *2016 ACC/AHA/HFSA Focused Update on New Pharmacological Therapy for Heart Failure: An Update of the 2013 ACCF/AHA Guideline for the Management of Heart Failure: A Report of the American College of Cardiology/American Heart Association Task Force on Clinical Practice Guidelines and the Heart Failure Society of America.* J Am Coll Cardiol, 2016. **68**(13): 1476-1488.

32. Ponikowski P, Voors A, Anker SD, Bueno H et al. *2016 ESC Guidelines for the diagnosis and treatment of acute and chronic heart failure: The Task Force for the diagnosis and treatment of acute and chronic heart failure of the European Society of Cardiology (ESC).* Eur Heart J, 2018. **37**(27): 2129-2200.

33. Ibanez B, James S, Agewall S, Antunes MJ, Bucciarelli-Ducci C, Bueno H, Caforio ALP, Crea F, Goudevenos JA, Halvorsen S, Hindricks G, Kastrati A, Lenzen ,MJ, Prescott E, Roffi M, Valgimigli M, Varenhorst C, Vranckx P, Widimský P; ESC Scientific Document Group . *2017 ESC Guidelines for the management of acute myocardial infarction in patients presenting with ST-segment elevation: The Task Force for the management of acute myocardial infarction in patients presenting with ST-segment elevation of the European Society of Cardiology (ESC)*. Eur Heart J. 2018. **39**(2):119-177

34. Mao AS, Mooney DJ. *Regenerative medicine: Current therapies and future directions*. Proc Natl Acad Sci U S A, 2015. **112**(47): 14452-9.

35. Fa-Ming Chen and Xiaohua Liu. *Advancing biomaterials of human origin for tissue engineering*. Prog Polym Sci, 2016. **53**: 86-168.

36. Sampogna G, Guraya SY, Forgione A. *Regenerative medicine: Historical roots and potential strategies in modern medicine*. J Microsc Ultrastruct, 2015. **3**: 101-107.

37. Sun R, Li X, Liu M, Zeng Y, Chen S and Zhang P. *Advances in stem cell therapy for cardiovascular disease*. Int J Mol Med, 2016. **38**: 23-29.

38. Malliaras K and Marban E. *Cardiac cell therapy: where we've been, where we are, and where we should be headed*. Br Med Bull, 2011. **98**: 161-185.

39. Taylor DA, Atkins BZ, Hungspreugs P, Jones TR, Reedy MC, Hutcheson KA, Glower DD and Kraus WE. *Regenerating functional myocardium: improved performance after skeletal myoblast transplantation*. Nat Med, 1998. **4**: 929-933.

40. Strauer BE, Brehm M, Zeus T, Köstering M, Hernandez A, Sorg RV, Kögler G and Wernet P. *Repair of infarcted myocardium by autologous intracoronary mononuclear bone marrow cell transplantation in humans*. Circulation, 2002. **106**: 1913-1918.

41. Traverse JH, Henry TD, Pepine CJ, Willerson JT, Zhao DX, Ellis SG, Forder JR, Anderson RD, Hatzopoulos AK, Penn MS, et al. *Cardiovascular Cell Therapy Research Network (CCTRN): Effect of the use and timing of bone marrow mononuclear cell delivery on left ventricular function after acute myocardial infarction: the TIME randomized trial*. JAMA, 2012. **308**: 2380-2389.

42. Sürder D, Schwitter J, Moccetti T, Astori G, Rufibach K, Plein S, Lo Cicero V, Soncin S, Windecker S, Moschovitis A, et al. *Cell-based therapy for myocardial repair in patients with acute myocardial infarction: rationale and study design of the SWiss multicenter Intracoronary Stem cells Study in Acute Myocardial Infarction (SWISS-AMI)*. Am Heart J, 2010. **160**: 58-64.

43. Davani S, Marandin A, Mersin N, Royer B, Kantelip B, Hervé P, Etievent JP and Kantelip JP. *Mesenchymal progenitor cells differentiate into an endothelial phenotype, enhance vascular density, and improve heart function in a rat cellular cardiomyo¬plasty model*. Circulation, 2003. **108 Suppl 1**: 253-258.

44. Sim EK, Haider HKh, Lila N, Schussler O, Chachques JC. *Genesis of myocardial repair with cardiac progenitor cells and tissue engineering*. Heart Asia, 2010. **2**(1):109-11.

45. Makkar RR, Smith RR, Cheng K, Malliaras K, Thomson LE, Berman D, Czer LS, Marbán L, Mendizabal A, Johnston PV, et al. *Intracoronary cardiosphere-derived cells for heart regen¬eration after myocardial infarction (CADUCEUS): a prospective, randomised phase 1 trial*. Lancet, 2012. **379**: 895-904.

46. Smith RR, Marban E and Marban L. *Enhancing retention and efficacy of cardiosphere-derived cells administered after myocardial infarction using a hyaluronan-gelatin hydrogel*. Biomatter, 2013. **3**: e24490.

47. Min JY, Yang Y, Converso KL, Liu L, Huang Q, Morgan JP and Xiao YF. *Transplantation of embryonic stem cells*

improves cardiac function in postinfarcted rats. J Appl Physiol (1985), 2002. **92**: 288-296.

48. Takahashi K, Tanabe K, Ohnuki M, Narita M, Ichisaka T, Tomoda K and Yamanaka S. *Induction of pluripotent stem cells from adult human fibroblasts by defined factors*. Cell, 2007. **131**: 861-872.

49. Takahashi K and Yamanaka S. *Induction of pluripotent stem cells from mouse embryonic and adult fibroblast cultures by defined factors*. Cell, 2006. **126**: 663-676.

50. Gerbin KA, Murry CE. *The winding road to regenerating the human heart*. Cardiovasc Pathol, 2015. **24**:133-40.

51. Ye L, Zimmermann WH, Garry DJ, Zhang J. *Patching the heart: cardiac repair from within and outside*. Circ Res, 2013. 113: 922-32.

52. O'Brien FJ. *Biomaterials & scaffolds for tissue engineering.* Mater Today, 2011. **14**: 88-95.

53. Stock UA, Vacanti JP. *Tissue engineering: current state and prospects*. Annu Rev Med, 2001. **52**: 443-51

54. Mikos AG, McIntire LV, Anderson JM, Babensee JE. *Host response to tissue engineered devices*. Adv Drug Deliv Rev, 1998. **33**(1-2): 111-139.

55. Chaudhuri R, Ramachandran M, Moharil P, Harumalani M, Jaiswal AK. *Biomaterials and cells for cardiac tissue engineering: Current choices*. Mater Sci Eng C Mater Biol Appl. 2017. **79**:950-957.

56. Engler AJ, Sen S, Sweeney HL, Discher DE. *Matrix elasticity directs stem cell lineage specification*. Cell, 2006. **126**(4): 677-89.

57. Badylak SF. *Decellularized allogeneic and xenogeneic tissue as a bioscaffold for regenerative medicine: factors that influence the host response*. Ann Biomed Eng, 2014. **42**(7):1517-27.

58. Keane TJ, Londono R, Turner NJ, Badylak SF. *Consequences of ineffective decellularization of biologic scaffolds on the host response*. Biomaterials, 2012. **33**(6): 1771-81.

59. Crapo PM, Gilbert TW, Badylak SF. *An overview of tissue and whole organ decellularization processes*. Biomaterials, 2011. **32**(12): 3233-43.

60. Di Meglio F, Nurzynska D, Romano V, Miraglia R, Belviso I, Sacco A, Barbato V, Di Gennaro M, Granato G, Maiello C, Montagnani S, Castaldo C. *Optimization of Human Myocardium Decellularization Method for the Construction of Implantable Patches*. Tissue Eng Part C Methods, 2017. **23**(9): 525-539.

61. Gilbert TW, Sellaro TL, Badylak SF. *Decellularization of tissues and organs*. Biomaterials, 2006. **27**(19): 3675-83.

62. Ahmed M, Ffrench-Constant C. *Extracellular Matrix Regulation of Stem Cell Behavior*. Curr Stem Cell Rep, 2016. **2**: 197-206.

63. Kular JK, Basu S, Sharma RI. *The extracellular matrix: Structure, composition, age-related differences, tools for analysis and applications for tissue engineering.* J Tissue Eng, 2014. **5**: 2041731414557112.

64. Frangogiannis NG. *The extracellular matrix in myocardial injury, repair, and remodeling*. J Clin Invest, 2017. **127**(5): 1600-1612.

65. Fukai K, Ishii M, Chanoki M, Kobayashi H, Hamada T, Muragaki Y, Ooshima A. *Immunofluorescent localization of type I and III collagens in normal human skin with polyclonal and monoclonal antibodies*. Acta Derm Venereol, 1988. **68**(3): 196-201.

66. Meigel WN, Gay S, Weber L. *Dermal architecture and collagen type distribution*. Arch Dermatol Res, 1977. **259**(1): 1-10.

67. Weber KT. *Cardiac interstitium in health and disease: the fibrillar collagen network*. J Am Coll Cardiol, 1989. **13**(7): 1637-52.

68. Joshi J, Mahajan G, Kothapalli CR. *Three-dimensional collagenous niche and azacytidine selectively promote time-dependent cardiomyogenesis from human bone marrow-derived MSC spheroids*. Biotechnol Bioeng, 2018. **115**(8): 2013-2026.

69. Mittal A, Pulina M, Hou SY, Astrof S. *Fibronectin and integrin alpha 5 play essential roles in the development of the cardiac neural crest*. Mech Dev, 2010. **127**(9-12):472-84.

70. Ando K, Takahashi M, Yamagishi T, Miyagawa-Tomita S, Imanaka-Yoshida K, Yoshida T, Nakajima Y. *Tenascin C may regulate the recruitment of smooth muscle cells during coronary artery development*. Differentiation, 2011. **81**(5):299-306

71. Hollfelder D, Frasch M, Reim I. *Distinct functions of the laminin β LN domain and collagen IV during cardiac extracellular matrix formation and stabilization of alary muscle attachments revealed by EMS mutagenesis in Drosophila*. BMC Dev Biol. 2014. **14**:26.

72. Wang X, Astrof S. Neural crest cell-autonomous roles of fibronectin in cardiovascular development. Development, 2016. **143**(1):88-100

73. Imanaka-Yoshida K, Yoshida T, Miyagawa-Tomita S. Tenascin-C in development and disease of blood vessels. Anat Rec (Hoboken), 2014. **297**(9):1747-57

74. Kim H, Yoon CS, Kim H, Rah B. Expression of extracellular matrix components fibronectin and laminin in the human fetal heart. Cell Struct Funct, 1999. **24**(1):19-26

75. Green EM, Mansfield JC, Bell JS, Winlove CP. *The structure and micromechanics of elastic tissue*. Interface Focus, 2014. **4**(2): 20130058.

76. Lindahl U. *A personal voyage through the proteoglycan field*. Matrix Biol, 2014. **35**: 3-7.

77. Theocharis AD, Skandalis SS, Gialeli C, Karamanos NK. *Extracellular matrix structure*. Adv Drug Deliv Rev, 2016. **97**: 4-27.

78. Nimeskern L, Utomo L, Lehtoviita I, Fessel G, Snedeker JG, van Osch GJ, Müller R, Stok KS. *Tissue composition regulates distinct viscoelastic responses in auricular and articular cartilage*. J Biomech 2016. **49**(3): 344-52.

79. Perie DS, Maclean JJ, Owen JP, Iatridis JC. *Correlating material properties with tissue composition in enzymatically*

digested bovine annulus fibrosus and nucleus pulposus tissue. Ann Biomed Eng, 2006. **34**(5): 769-77.

80. Qiu Y, Bayomy AF, Gomez MV, Bauer M, Du P, Yang Y, Zhang X, Liao R. *A role for matrix stiffness in the regulation of cardiac side population cell function*. Am J Physiol Heart Circ Physiol, 2015. **308**(9): H990-7.
81. Gallina C, Dolgetta S, Alloatti G, Levi R, Gallo MP. *Development of morphology and function of neonatal mouse ventricular myocytes cultured on a hyaluronan-based polymer scaffold*. J Cell Biochem, 2012. **113**(3): 800-7.
82. Thimm TN, Squirrell JM, Liu Y, Eliceiri KW, Ogle BM. *Endogenous Optical Signals Reveal Changes of Elastin and Collagen Organization During Differentiation of Mouse Embryonic Stem Cells*. Tissue Eng Part C Methods, 2015. **21**(10):995-1004.
83. Hanson KP, Jung JP, Tran QA, Hsu SP, Iida R, Ajeti V, Campagnola PJ, Eliceiri KW, Squirrell JM, Lyons GE, Ogle BM. *Spatial and temporal analysis of extracellular matrix proteins in the developing murine heart: a blueprint for regeneration*. Tissue Eng Part A, 2013. **19**(9-10): 1132-43.
84. Kim KH, Nakaoka Y, Augustin HG, Koh GY. *Myocardial Angiopoietin-1 Controls Atrial Chamber Morphogenesis by Spatiotemporal Degradation of Cardiac Jelly*. Cell Rep, 2018. **23**(8): 2455-2466.
85. Farouz Y, Chen Y, Terzic A, Menasché P. *Concise review: growing hearts in the right place: on the design of biomimetic materials for cardiac stem cell differentiation*. Stem Cells, 2015. **33**(4):1021-35.

86. Terzini M, Aldieri A, Castaldo C, Di Meglio F, Nurzynska D, Serino G, Audenino AL, Massai D. *Mechanical behaviour of human decellularized dermis as scaffold for myocardial regeneration*. 8th World Congress of Biomechanics, 2018, Dublin, Ireland.

87. Massai D, Terzini M, Aldieri A, Romano V, Castaldo C, Di Meglio F , Nurzynska D, Serino G, Bignardi C, Audenino A. *Human Decellularized Dermis as Biological Scaffold for Myocardial Regeneration: Mechanical Characterization*. 5th TERMIS WORLD CONGRESS 2018, KYOTO, JAPAN.

88. Camenisch TD, Spicer AP, Brehm-Gibson T, Biesterfeldt J, Augustine ML, Calabro A Jr, Kubalak S, Klewer SE, McDonald JA. *Disruption of hyaluronan synthase-2 abrogates normal cardiac morphogenesis and hyaluronan-mediated transformation of epithelium to mesenchyme*. J Clin Invest, 2000. **106**(3): 349-60.

89. Vasita R, Katti DS. *Growth factor-delivery systems for tissue engineering: a materials perspective.* Expert Rev Med Devices, 2006, 3(1):29-47

90. Yue, B. *Biology of the extracellular matrix: an overview*. J. Glaucoma, 2014. **23**: 20–23.

91. Gallo S, Sala V, Gatti S, Crepaldi T. *HGF/Met Axis in Heart Function and Cardioprotection*. Biomedicines, 2014. **2**(4): 247-262.

92. Sala V, Crepaldi T. *Novel therapy for myocardial infarction: can HGF/Met be beneficial?* Cell Mol Life Sci, 2011. **68**(10): 1703-17.

93. Madonna R, Rokosh G, De Caterina R, Bolli R. *Hepatocyte growth factor/Met gene transfer in cardiac stem cells--potential for cardiac repair*. Basic Res Cardiol, 2010. **105**(4): 443-52.

94. Farzaneh M, Rahimi F, Alishahi M, Khoshnam SE. *Paracrine mechanisms involved in mesenchymal stem cell differentiation into cardiomyocytes*. Curr Stem Cell Res Ther, 2018. doi: 10.2174/1574888X1366180821160421.

95. Ma J, Zhao Y, Sun L, Sun X, Zhao X, Sun X, Qian H, Xu W, Zhu W. *Exosomes Derived from Akt-Modified Human Umbilical Cord Mesenchymal Stem Cells Improve Cardiac Regeneration and Promote Angiogenesis via Activating Platelet-Derived Growth Factor D*. Stem Cells Transl Med, 2017. **6**(1): 51-59.

96. Lewis FC, Kumar SD, Ellison-Hughes GM. *Non-invasive strategies for stimulating endogenous repair and regenerative mechanisms in the damaged heart*. Pharmacol Res, 2018. **127**: 33-40.

97. Vandervelde S, van Luyn MJ, Tio RA, Harmsen MC. *Signaling factors in stem cell-mediated repair of infarcted myocardium.* J Mol Cell Cardiol, 2005. **39**(2): 363-76.

98. Troncoso R, Ibarra C, Vicencio JM, Jaimovich E, Lavandero S. *New insights into IGF-1 signaling in the heart*. Trends Endocrinol Metab, 2014. **25**(3): 128-37.

99. Sun Y, Han X, Wang X, Zhu B, Li B, Chen Z, Ma G, Wan M. *Sustained Release of IGF-1 by 3D Mesoporous Scaffolds Promoting Cardiac Stem Cell Migration and Proliferation*. Cell Physiol Biochem, 2018. **49**(6): 2358-2370.

100. Kusano K, Tsutsumi Y, Dean J, Gavin M, Ma H, Silver M, Thorne T, Zhu Y, Losordo DW, Aikawa R. *Long-term stable expression of human growth hormone by rAAV promotes myocardial protection post-myocardial infarction*. J Mol Cell Cardiol, 2007. **42**:390-9

101. Saetrum Opgaard O, Wang PH. *IGF-1 is a matter of heart*. Growth Horm IGF Res. 2005. **15**(2):89-94

102. Aghila Rani KG, Kartha CC. *Effects of epidermal growth factor on proliferation and migration of cardiosphere-derived cells expanded from adult human heart*. Growth Factors, 2010. **28**(3):157-65

103. Schwarz B, Hollfelder D, Scharf K, Hartmann L, Reim I. *Diversification of heart progenitor cells by EGF signaling and differential modulation of ETS protein activity*. Elife, 2018. **7**. pii: e32847

104. Deshwar AR, Chng SC, Ho L, Reversade B, Scott IC. *The Apelin receptor enhances Nodal/TGFβ signaling to ensure proper cardiac development.* Elife, 2016. **5**. pii: e13758

105. Qiu C, Xie Q, Zhang D, Chen Q, Hu J, Xu L. *GM-CSF induces cyclin D1 expression and proliferation of endothelial progenitor cells via PI3K and MAPK signaling*. Cell Physiol Biochem, 2014. **33(3)**:784-95.

106. Zhu H, Li X, Yuan M, Wan W, Hu M, Wang X, Jiang X. *Intramyocardial delivery of bFGF with a biodegradable and thermosensitive hydrogel improves angiogenesis and cardio-protection in infarcted myocardium*. Exp Ther Med, 2017. **14(4)**:3609-3615.

107. Fu JD, Srivastava D. *Direct reprogramming of fibroblasts into cardiomyocytes for cardiac regenerative medicine*. Circ J, 2015. **79(2)**:245-54.

List of publications

1. Sacco AM, Belviso I, Romano V, Carfora A, Schonauer F, Nurzynska D, Montagnani S, Di Meglio F, **Castaldo C**. Diversity of dermal fibroblasts as major determinant of variability in cell reprogramming. **J Cell Mol Med**. (*Under review).*
2. Sirico F, **Castaldo C**, Baioccato V, Marino N, Zappia M, Montagnani S, Di Meglio F, Nurzynska D. Prevalence of musculocutaneous nerve variations: systematic review and meta-analysis. **Clin Anat**. **2018** Aug 16. doi: 10.1002/ca.23256. [Epub ahead of print] Review.
3. Boffito M, Di Meglio F, Mozetic P, Giannitelli SM, Carmagnola I, **Castaldo C**, Nurzynska D, Sacco AM, Miraglia R, Montagnani S, Vitale N, Brancaccio M, Tarone G, Basoli F, Rainer A, Trombetta M, Ciardelli G, Chiono V. Surface functionalization of polyurethane scaffolds mimicking the myocardial microenvironment to support cardiac primitive cells. **PLoS One**. **2018** Jul 6; 13(7):e0199896. doi: 0.1371/journal.pone.0199896. eCollection 2018.
4. Sirico F, Bianco A, D' Alicandro G, **Castaldo C**, Montagnani S, Spera R, Di Meglio F, Nurzynska D. Effects of Physical Exercise on Adiponectin, Leptin, and Inflammatory Markers in Childhood Obesity: Systematic Review and Meta-Analysis. **Child Obes**. **2018** May/Jun; 14(4):207-217. doi: 10.1089/chi.2017.0269. Epub 2018 May 15.
5. **Castaldo C**, Chimenti I. Cardiac Progenitor Cells: The Matrix Has You. **Stem Cells Transl Med**. **2018** Apr 24. doi: 10.1002/sctm.18-0023.
6. Sirico F, Miressi S, **Castaldo C**, Spera R, Montagnani S, Di Meglio F, Nurzynska D. Habits and beliefs related to food

supplements: Results of a survey among Italian students of different education fields and levels. **PLoS One**. **2018** Jan 19; 13(1):e0191424. doi: 10.1371/journal.pone.0191424. eCollection 2018.

7. Iaconetta G, Solari D, Villa A, **Castaldo C**, Gerardi RM, Califano G, Montagnani S, Cappabianca P. The Hypoglossal Nerve: Anatomical Study of Its Entire Course. **World Neurosurg**. **2018** Jan; 109:e486-e492. doi: 10.1016/j.wneu.2017.10.006. Epub 2017 Oct 12.

8. Pagano F, Angelini F, **Castaldo C**, Picchio V, Messina E, Sciarretta S, Maiello C, Biondi-Zoccai G, Frati G, Di Meglio F, Nurzynska D, Chimenti I. Normal versus Pathological Cardiac Fibroblast-Derived Extracellular Matrix Differentially Modulates Cardiosphere-Derived Cell Paracrine Properties and Commitment. **Stem Cells Int. 2017**; 2017:7396462. doi: 10.1155/2017/7396462. Epub 2017 Jun 27.

9. Di Meglio F, Nurzynska D, Romano V, Miraglia R, Belviso I, Sacco AM, Barbato V, Di Gennaro M, Granato G, Maiello C, Montagnani S, **Castaldo C**. Optimization of Human Myocardium Decellularization Method for the Construction of Implantable Patches. **Tissue Eng Part C Methods. 2017** Sep; 23(9):525-539. doi: 10.1089/ten.TEC.2017.0267. Epub 2017 Aug 10.

10. Sirico F, Ricca F, DI Meglio F, Nurzynska D, **Castaldo C**, Spera R, Montagnani S. Local corticosteroid versus autologous blood injections in lateral epicondylitis: meta-analysis of randomized controlled trials. **Eur J Phys Rehabil Med. 2017** Jun; 53(3):483-491. doi: 10.23736/S1973-9087.16.04252-0. Epub 2016 Sep 1. Review.

11. Puzzo D, Raiteri R, **Castaldo C**, Capasso R, Pagano E, Tedesco M, Gulisano W, Drozd L, Lippiello P, Palmeri A, Scotto P, Miniaci MC. CL316,243, a β3-adrenergic receptor agonist, induces muscle hypertrophy and increased strength. **Sci Rep**. **2016** Nov 22; 5:37504. doi: 10.1038/srep37504.

12. Nappi F, Fraldi M, Spadaccio C, Carotenuto AR, Montagnani S, **Castaldo C**, Chachques JC, Acar C. Biomechanics drive histological wall remodeling of neoaortic root: A mathematical model to study the expression levels of ki 67, metalloprotease, and apoptosis transition. **J Biomed Mater Res A**. **2016** Nov; 104(11):2785-93. doi: 10.1002/jbm.a.35820.

Congress communications

1. **Castaldo C**, Di Meglio F, Belviso I, Sacco AM, Carfora A, Romano V, Massai D, Nurzynska D, Schonauer F, Montagnani S. Scaffold of decellularized human dermis for cardiac repair and regeneration. 72th Meeting of the Italian Society of Anatomy and Histology**. It J Anat Embryol**, Vol.123, n.1 (Supplement):50, 2018.

2. **Castaldo C**, Di Meglio F, Romano V, Schonauer F, Massai D, Belviso I, Nurzynska D, Sacco AM, Di Gennaro M, Carfora A, Avagliano A, Montagnani S. Decellularized Human Skin As Biological Scaffold for the Regeneration of Human Heart By Resident Cardiac Progenitor Cells. **5th TERMIS WORLD CONGRESS 2018, KYOTO, JAPAN.**

3. Massai D, Terzini M, Aldieri A, Romano V, **Castaldo C**, Di Meglio F, Nurzynska D, Serino G, Bignardi C, Audenino A. Human Decellularized Dermis as Biological Scaffold for Myocardial Regeneration: Mechanical Characterization. **5th TERMIS WORLD CONGRESS 2018, KYOTO, JAPAN.**

4. Chiono V, Paoletti C, Divieto C, Di Meglio F, **Castaldo C,** Nurzynska D. Direct cell reprogramming as a new emerging strategy in cardiac regeneration. **5th TERMIS WORLD CONGRESS 2018, KYOTO, JAPAN .**

5. **Castaldo C**, Nurzynska D, Romano V, Sacco A, Belviso I, Di Gennaro M, Carfora A, Avagliano A, Schonauer F, Montagnani S, Di Meglio F. From Cover to Core: Acellular Human Dermis for the Regeneration of Human Heart.2017 TERMIS - Americas Conference & Exhibition. **TISSUE ENGINEERING: Part A,** Vol. 23 (Supplement 1): S-67, 2017.

6. Romano V, Di Meglio F, Nurzynska D, Belviso I, Sacco A, Di Gennaro M, Carfora A, Avagliano A, Greco L, Montagnani S, **Castaldo C**. Optimization of Human Heart Decellularization Method. 2017 TERMIS - Americas Conference & Exhibition. **TISSUE ENGINEERING: Part A,** Vol. 23 (Supplement 1): S-68, 2017.

7. Sacco A, Di Meglio F, Nurzynska D, Romano V, Belviso I, Di Gennaro M, Carfora A, Avagliano A, Greco L, Schonauer F, Montagnani S, **Castaldo C**. Fibroblast Looks Like a Mesenchymal Stem Cell and Talks Like a Mesenchymal Stem Cell: is It a Mesenchymal Stem Cell in Disguise? 2017 TERMIS – Americas Conference & Exhibition. **TISSUE ENGINEERING: Part A,** Vol. 23 (Supplement 1): S-112, 2017.

8. Romano V, Di Meglio F, Nurzynska D, Belviso I, Sacco AM, Di Gennaro M, Carfora A, Avagliano A, Greco L, Montagnani S, **Castaldo C**. Optimization Of Human Heart Decellularization Method For Cardiac Regenerative Medicine. 71st Meeting of the Italian Society of Anatomy and Histology. **Ital J Anat Embryol**, Vol. 122(1Suppl):184, 2017.

9. Cerrone A, Tuzi M, Postiglione A, Sirico F, Di Meglio F, **Castaldo C,** Montagnani S. Rectus femoris proximal insertion

anatomy - analysis of the clinically relevant anatomy and variations. 71st Meeting of the Italian Society of Anatomy and Histology. **Ital J Anat Embryol**, Vol. 122(1Suppl):59, 2017.

10. **Castaldo C**, Nurzynska D, Romano V, Belviso I, Sacco AM, Carfora A, Di Gennaro M, Greco L, Schonauer F, Montagnani S, Di Meglio F. Decellularized human skin as biological scaffold for cardiovascular repair and regeneration. **28th Annual Conference of the European Society for Biomaterials (ESB)**, Athens, Greece, Sep 04-08, 2017.
11. Di Meglio F, Schonauer F, Nurzynska D, Romano V, Belviso I, Miraglia R, Granato G, Sacco A, Carfora A, Di Gennaro M, Barbato V, Montagnani S, **Castaldo C**. Relevance of Positional Memory of Fibroblasts in Reprogramming to Induced Pluripotent Stem Cells. 2016 TERMIS - Americas Conference & Exhibition. **TISSUE ENGINEERING: Part A**, Vol. 22 (Supplement 1): S-3, 2016.
12. Romano V, Miraglia R, Di Meglio F, Nurzynska D, Belviso I, Sacco A, Di Gennaro M, Barbato V, Granato G, Carfora A, Montagnani S, **Castaldo C**. Struggling to Prepare an Injectable Self-Assembling Human Cardiac Matrix and Facing Unexpected Failure. 2016 TERMIS - Americas Conference & Exhibition. **TISSUE ENGINEERING: Part A**, Vol. 22 (Supplement 1): S-47, 2016.
13. Belviso I, **Castaldo C**, Nurzynska D, Romano V, Miraglia R, Granato G, Sacco A, Carfora A, Greco L, Barbato V, Di Gennaro M, Montagnani S, Di Meglio F. Exosomes Delivered by Human Cardiac Primitive Cells Impact on Both Cardiac Cellular and Extracellular Compartment. 2016 TERMIS - Americas Conference & Exhibition. **TISSUE ENGINEERING: Part A**, Vol. 22 (Supplement 1): S-110, 2016.
14. Sacco A, Di Meglio F, Nurzynska D, Miraglia R, Romano V, Barbato V, Belviso I, Di Gennaro M, Granato G, Carfora A,

Montagnani S, **Castaldo C**. Fibrin and Extracellular Matrix As in Vivo Self-Assembling Scaffold for Direct Delivery of Cardiac Primitive Cells. 2016 TERMIS - Americas Conference & Exhibition. **TISSUE ENGINEERING: Part A**, Vol. 22 (Supplement 1): S-120, 2016.

15. Nurzynska D, **Castaldo C**, Di Meglio F, Mozetic P, Giannitelli SM, Rainer A, Brancaccio M, Vitale N, Boffito M, Carmagnola I, Ciardelli G, Chiono V. Functionalised polyurethane scaffolds mimicking cardiac primitive cell niche microenvironment by additive manufacturing. 2016 TERMIS - EU Conference. **European Cells and Materials**, Vol. 31 (suppl.1): 162, 2016.
16. **Castaldo C**, Di Meglio F, Nurzynska D, Barbato V, Belviso I, Di Gennaro M, Romano V, Miraglia R, Sacco AM, Granato G, Montagnani S. Decellularized human cardiac extracellular matrix as a natural scaffold for stem cell-based cardiac engineering. 10th World Biomaterials Congress, 2016. **Front. Bioeng. Biotechnol.** Conference Abstract: 10th World Biomaterials Congress, 2016. doi: 10.3389/conf.FBIOE.2016.01.00619.
17. Romano V, Carfora A, Miraglia R, Belviso I, Barbato V, Sacco AM, Granato G, Di Gennaro M, Di Meglio F, **Castaldo C**, Nurzynska D, Montagnani S. Positional memory of fibroblast may affect efficiency of iPSC reprogramming. 70º Congresso della Società Italiana di Anatomia e Istologia, 2016. **It J Anat Embryol**, Vol. 121, n.1 (Supplement): 171, 2016.
18. Belviso I, Di Gennaro M, Romano V, Miraglia R, Barbato V, Sacco AM, Granato G, Di Meglio F, Nurzynska D, Montagnani S, **Castaldo C**. Identifying the ideal somatic cell for direct cardiac progenitor reprogramming. **15th World Stem cell summit** 2015, Atlanta, GA, USA.

19. **Castaldo C**, Nurzynska D, Belviso I, Barbato V, Di Gennaro M, Romano V, Miraglia R, Sacco AM, Granato G, Montagnani S, Di Meglio F. Development of bioconstructs of human myocardium to enable cardiac regeneration. **15th World Stem cell summit** 2015, Atlanta, GA, USA.

20. Nurzynska D, Di Meglio F, Sacco AM, Granato G, Belviso I, Barbato V, Di Gennaro M, Romano V, Miraglia R, Vitale M, Zambrano N, Scaloni A, Renzone G, Montagnani S, **Castaldo C**. In Vitro Produced Cardiac Extracellular Matrix for Studies of Myocardium Regeneration Potential. 4th TERMIS World Congress, 2015. **TISSUE ENGINEERING: Part A**, Vol. 21, Supplement 1: S-77, 2015.

21. Chiono V, Boffito M, Sartori S, Gioffredi E, Massai D, Mozetic P, Giannitelli S, Rainer A, Trombetta M, **Castaldo C**, Nurzynska D, Di Meglio F, Miraglia R, Montagnani S, Vitale N, Tarone G, Ciardelli G. Biomimetic Polyurethane Scaffolds Guiding the In Vitro Behavior of Cardiac Stem Cells; 4th TERMIS World Congress, 2015. **TISSUE ENGINEERING: Part A,** Vol. 21 (Supplement 1): S-312, 2015.

Acknowledgements

I am extremely grateful to all the people I met, and I got to know thus far, as I firmly believe they all contributed to make me become the person I am, and they unconsciously guided me along my path.

I wish to thank my family for constant support and trust and my friends, the few true ones, for their silent but still heart-felt presence. Among all, I have to thank my mother for teaching me that commitment is key to achievement and for being my beacon through all these years, my siblings and nieces for their endearing questions about my research that made me understand how hard it is to talk to broader audience and how important it is to share our thoughts and doubts, my friend and colleague Franca who was by my side for more than two decades and respected all the decisions I made supporting me without intrusions, my labmates and friends Anna Maria, Titti and Veronica for their invaluable expertise and loyalty through the years.

A special thanks to Cindy, my dog and life companion who silently stands by my side and fills my days with joy and unconditional love like no one else.

Furthermore, I am profoundly grateful to Professor Stefania Montagnani, my tutor and passionate supporter, Professors and Coordinators of the PhD School Sergio Adamo and Antonio Musarò who granted me the chance to further learning and, together with Professor Carla Boitani, undertook the fruitful discussion that led to the exciting results I obtained through these three years by stimulating the implementation of my research project.

Finally, I am to recognize that without the knowledgeable contribution of Professors Giulia Ricci and Angiolina Catizone and their coworkers this research would lack some of the evidence that turned them into two of the most enthusiastic true believers of the potential powerful impact of my findings on cardiac regenerative medicine applications.